國 立 交 通 大 學

電子工程學系電子研究所碩士班

碩 士 論 文

氮化鋁鎵/氮化鎵高電子遷移率電晶體之銅金屬化製程研究

The Study of Copper Metallization for AlGaN/GaN High Electron Mobility Transistors

研 究 生：張羅衡

指導教授：施敏、張翼 教授

中華民國一百零一年三月

氮化鋁鎵/氮化鎵高電子遷移率電晶體之銅金屬化製程研究

The Study of Copper Metallization for AlGaN/GaN High Electron Mobility Transistors

研　究　　生：張羅衡　　　　　　　　　　Student：Lo-Heng Chang

指　導　教　授：施敏、張翼　　　　　　　　Advisor：Dr. Simon M. Sze

Dr. Edward Yi Chang

國　立　交　通　大　學

電子工程學系電子研究所碩士班

碩　士　論　文

A Thesis
Submitted to Department of Electronics Engineering
College of Electrical Electronics Engineering
National Chiao Tung University
in Partial Fulfillment of the Requirements
for the Degree of
Master
in

Electronics Engineering

March 2012

Hsinchu, Taiwan, Republic of China

中華民國 一百零一 年　三 月

氮化鋁鎵/氮化鎵高電子遷移率電晶體之銅金屬化製程研究

研究生：張羅衡　　　　　　　　　　　　　　　指導教授：施敏、張翼

摘要

　　氮化鎵元件在高功率和高頻的應用一直備受矚目。然而為了增加市場佔有率，製程成本必須達到最小化，而氮化鎵元件常使用金來做金屬接觸是高製造成本的原因之一。本實驗即研究利用銅金屬化製程取代傳統使用金的製程，來降低製造成本。

　　首先使用鈦鋁鎢取代傳統的鈦鋁鎳金歐姆接觸，製作不同厚度的鈦然後在不同的溫度下退火，以期找到降低特徵接觸電阻的最佳條件，並利用多重步驟退火的方法進一步降低阻值，接著藉由 X 光繞射、原子力學顯微鏡、及穿透式電子顯微鏡做材料分析，實驗所得最佳的特徵接觸電阻為 $2 \times 10^{-5} \; \Omega \; cm^2$，而且有極佳的表面平整度。

　　蕭基接觸的金屬則是利用氮化鎢/銅來取代鎳/金。氮化鎢/銅閘極的漏電流約為鎳/金閘極漏電流的十分之一，實驗所得之理想係數為 1.57，蕭基能障高度為 0.67ev。光罩圖形經過特別設計使得進行氮化鎢閘極製作時同時沉積氮化鎢於鈦/鋁/鎢歐姆接觸上，接著製作具有傳統鈦/鋁/鎳/金歐姆接觸以及鎳/金閘極的元件來比較其電性。

　　銅金屬化的元件的崩潰電壓為 125V 飽和電流密度為 420mA/mm，轉導為 190ms/mm，元件特性和傳統使用金製程的元件相當，說明本研究在矽基板上成功開發不使用金而用銅的氮化鋁鎵/氮化鎵高遷移率電晶體之低成本製程。

Copper Metallization Study of AlGaN/GaN High Electron Mobility Transistors

Student: Lo-Heng Chang   **Advisor: Dr. Simon M. Sze**

Dr. Edward Yi Chang

Department of Electronics Engineering

Abstract

GaN has drawn much attention for high power and high frequency applications. In order to increase the market share, the costs of process have to be minimized. Gold based metallization is usually used for GaN devices and that is one of the reasons responsible for high processing cost. To replace traditional gold metallization on GaN, copper metallization was studied. The processing cost could be significantly reduced with copper metallization.

Instead of the traditional Ti/Al/Ni/Au, Ti/Al/W was used for ohmic contacts. Different thicknesses of Ti layer and rapid thermal annealing temperatures are tested to obtain the lowest specific contact resistivity. The results were further improved with multi-step annealing process. X-ray diffraction, atomic force microscopy and transmission electron microscopy were used for material analysis. A specific contact resistivity of 2×10^{-5} Ω cm^2 was obtained with excellent surface morphology.

Instead of Ni/Au, WNx/Cu was used for Schottky contact metal. The leakage current of WNx/Cu gates were about one order lower than that for Ni/Au. An ideality factor of 1.57 and a Schottky barrier height of 0.67ev were obtained. With the special design of mask, WNx/Cu was deposited on the top of Ti/Al/W ohmic contacts the same time with gate patterning. Devices with traditional Ti/Al/Ni/Au ohmic and Ni/Au gate were also prepared for comparison.

The HEMT devices with copper metallization exhibited breakdown voltage of 125V. The saturation current is 420mA/mm and the maximum transconductance is 190ms/mm. These results are comparable with gold based devices. Therefore, the low cost process with copper metallization and not involving gold metallurgy for AlGaN/GaN HEMTs are successfully developed.

Contents

Chapter 4

Fabrication of AlGaN/GaN high electron mobility transistor with copper metallization process

Chapter 5

Table Captions

Chapter 2

Figure Captions

.

Chapter 4

Chapter 1

Introduction

1-1 GaN based devices

Recently, the smart phone and hand mobile electronics develop rapidly. The consumer demands increase in wireless industry with exploding data transferring needs. These needs will drive the progression of wireless industry from 3G to 4G. result in the need of high performance RF and microwave devices increasing steadily. More power, more frequency bands, better linearity and improved efficiency are driving the development of RF semiconductor devices capable of handling all these specifications at a reasonable price.

GaN HEMT has drawn much attention because it has high electron mobility, high saturation velocity and high breakdown voltage. These properties make it a strong candidate for wireless base station amplifiers, radars, high frequency and high power devices application. The high power per unit width translates into smaller devices could offer higher impedance and also make them easier to make. Higher impedance makes GaN based devices much easier to match to the system, which is often a complicated task with conventional GaAs based devices.

1-2 Motivation

The needs in commercial, defense, and communication system keep driving the performance of GaN based devices. Although GaN benefits from its superior material properties the cost structure are not as good as Si based devices. In order to get higher market share, it is imperative to minimize devices fabrication costs. With the technology of growing GaN on Si substrate become mature. The cost for fabrication

was cut down significantly. There is still a big room for cost down with metallization process in addition to realizing low costs for substrates and epitaxial layers. Gold metallization has taken a major part in processing cost. There are mainly three parts of GaN devices with gold metallization, ohmic, gate, and airbridge. Finding a metal system to replace gold will make GaN based devices more competitive at price which helps GaN to get higher market share. Copper is a good choice to replace gold due to its electrical properties and cheap price. But copper has reliability issues and need the design of diffusion barrier. This study tried to replace gold metallization with designed diffusion barrier to reduce the manufacturing costs.

Chapter2

AlGaN/GaN High Electron Mobility Transistors

2-1 Material properties of GaN

GaN is the next important semiconductor material after Si and GaAs. III-V nitride materials show many special properties compare to SiAmong these GaN draws increasing attention for a wide range of device applications, including high power, high frequency, high temperature electronic devices.

GaN is a hard and stable material with Wurtzite crystal or Zinc-blend structure. It can be deposited as a thin film on proper substrates. The basic material properties are shown in Table. 2-1.

The wide band gap of GaN leads to very high breakdown fields(1.5×10^7V/m as compared to 2.5×10^5V/m for GaAs).This allows GaN to be biased at very high drain voltages. Moreover, the wide band gap also leads to the low intrinsic carrier concentration for wide range of temperature. This allows GaN devices to be operated at high temperature. Since GaN transistors can operate at much hotter temperatures and work at much higher voltages than GaAs transistors, they can make ideal power amplifiers at microwave frequencies.
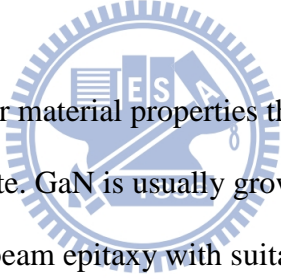
Although the mobility of GaN is not very high, it is less sensitive to ionized impurity concentration. It also has larger peak velocity than GaAs which gives GaN capable to high current and high frequency operation.

High thermal conductivity of GaN allows channel temperature to reach 300^oC. And the stability in radiation makes GaN a candidate to military and satellite application. GaN based devices will play an important role for high power, high temperature, and high frequency applications.

2-2 AlGaN/GaN high electron mobility transistors

Fig. 2-1. shows the structure of GaN HEMT. The energy bandgap difference between AlN and GaN permits high concentrations of free carriers to be confined at the AlGaN/GaN heterointerface. The electrons diffuse from the large bandgapAlGaN into the smaller bandgap GaN and form a two-dimensional electron gas(2DEG) in the triangle quantum well at the interface paving the way for the high-performance AlGaN/GaN high-electron mobility transistors (HEMT).

2-3 The choice of GaN substrate

Although GaN has superior material properties the commercial applications are limited by the choice of substrate. GaN is usually grown by metal organic chemical vapor deposition or molecular beam epitaxy with suitable substrates. The properties of substrate commonly used are listed in Table. 2-2. Sapphire was first used to grow GaN. With the development of growing techniques, the lattice mismatch between GaN and sapphire could be solved by low temperature buffer layer. But low thermal conductivity still limits the application of sapphire. SiC has less lattice mismatch and very good thermal conductivity compare to sapphire. But the price of SiC is too expensive. As the growing techniques getting mature, Si become a popular choice of the substrates because of it's low cost and mature process technology.

.Figures

SiN Passivation

SOURCE GATE DRAIN

AlGaN

2DEG GaN

Nucleation
Layer
GaN, AlGaN or AlN

Substrate: Typically Sapphire or SiC

2DEG

E_C
E_F

AlGaN **GaN**

E_V
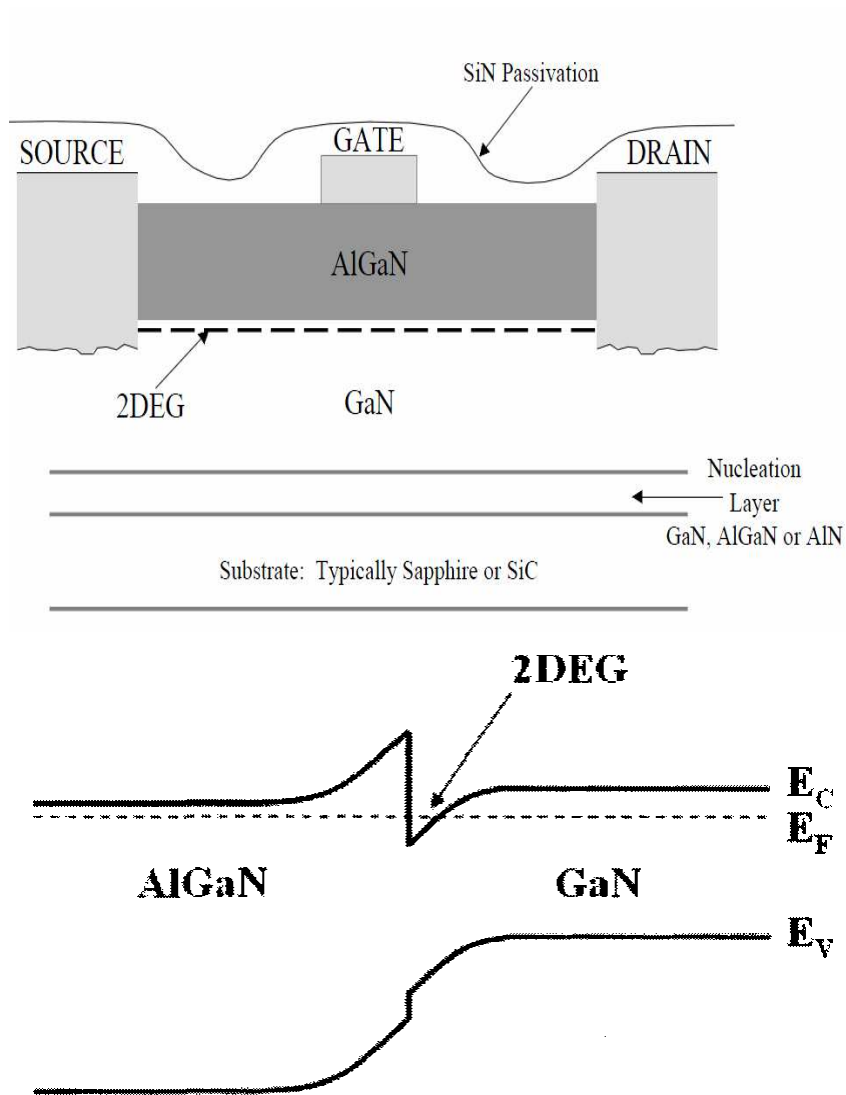
Fig. 2-1 Cross-sectional view of AlGaN/GaN HEMT and
band diagram.
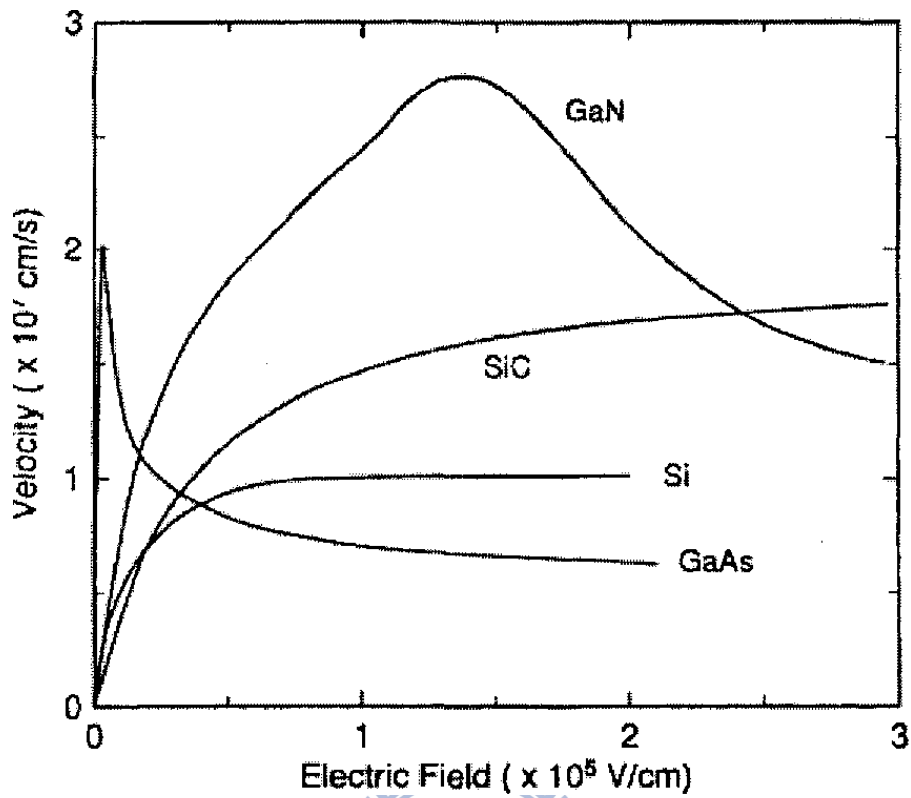
Fig.2-2 Material properties of GaN, SiC and GaAs.
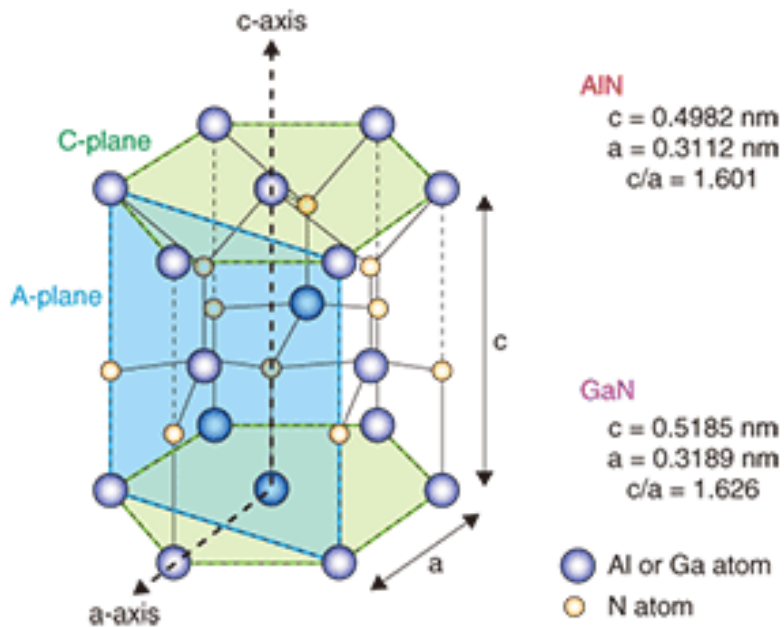
Fig.2-3 Schematic drawing of the wurtzite GaN crystal
structure

Material	Mobiltiy $(cm^2/V \times S)$	Saturated velocity $(\times 10^7 \text{ cm/s})$	Band gap (ev)	Breakdown voltage (MV/cm)	Thermal conductivity $(W/cm \times K)$
GaN	800	2.7	3.4	3.3	1.3
GaAs	8500	2.0	1.4	0.4	0.5
Si	1300	1.0	1.1	0.3	1.5

Table 2-1 Material propertied of GaN, Si, and GaAs

Substrate	Lattice Constant(Å)	Lattice mismatch(%)	σ_T (W/cm-K)	TCE(10^{-6}/K)
Sapphire	2.747	13.9	0.5	7.5
Si	5.430	-70.3	1.5	3.6
SiC	3.080	3.4	4.9	4.2

Table 2-2 Properties of substrate used for GaN Growth..

Chapter 3

Fabrication of Ti/Al/W ohmic contacts for AlGaN/GaN heterostructure

3-1 Introduction

Ohmic contacts are the contacts of metal/semiconductor which have very low resistance. Low resistance ohmic contacts play a crucial role of GaN devices for many applications. High performance microwave devices require ohmic contact with specific contact resistivity lower than $10^{-5} \, \Omega \, \text{cm}^2$.

Large band gap gives GaN superior material properties but also makes forming low resistance ohmic contact on it become very challenge. Most of the ohmic contacts developed contain two metals. Ti and Al. The contact structures include Ti-only, Al-only, Ti/Al/Ni/Au[1,2], Ti/Al/Mo/Au[3], Ti/Al/Pt/Au[4, 5] and Ti/Al/Ti/Au[6]. Ti-only and Al-only ohmic contacts have oxide penetration problems. With higher operation temperature the oxidation of ohmic contacts causes reliability issues. The low melting temperature of Al is another problem for thermal reliability of Ti/Al contacts. Since the RTA temperature of ohmic contacts usually higher than 800C, the Al tends to ball up and make the surface morphology become rough. Gold is usually used as a cap layer for the ohmic contacts to prevent oxide penetration. But diffusion of gold into GaN will cause long term reliability issues. A diffusion barrier layers is used between Al and gold such as Ni, Ti, Pd and Pt.

Ti based ohmic contacts could form TiN interfacial layer with GaN. This results in vacancies in GaN. Al and Ti are both easily oxide in air. Au was used as a cap layer to prevent Al and Ti from oxidation. Research shows when gold diffuse into Al will cause long term reliability issues. Ni is used as diffusion layer to prevent gold from

diffuse into Al.

3-2 Design rules of ohmic contacts

The basic design principles for ohmic contacts on GaN need four layers M1, M2, M3 and M4. First layer M1 must have low resistance and small work function and it also must form stable metallic alloy with GaN. For low specific contact resistance, M1 must react with GaN to form M1N compound. The M1N consume the nitrogen of GaN and leave behind N vacancies. The vacancies are known to act as n-type dopant atoms. The band gap level of these vacancies is very close to the conduction band edge of n GaN. The choice of M1 is usually one of Ti, Zr, Ta, Co, etc. The M1 layer has two important tasks: First, it have to form a thermal stable metallic compound layer with GaN and M2, and second it must create high density of N vacancies in GaN layer.

Most of the low resistance ohmic contacts have M2 layer on M1. This layer can help M1 to consume N atoms. The formation of M1M2N create more N vacancies than M1 only. Al is a good choice for M2 layer as long as it doesn't have large work function alloy.

For some conditions, M1 and M2 layers have oxidation problems. That's why the M3 and M4 are necessary. M4 layer serve as a cap layer on the top of the ohmic structure. This layer must able to prevent the oxide penetration. And the alloy system of M1, M2, M4 must not let M1 M2 out diffuse from M4.

M3 layer act as a diffusion barrier layer to prevent the M4 diffuse into GaN layer. It also has increase the adhesion between M3 and M4. The existence of M3 makes the whole alloy system become more stable and reduce the total free energy.

After the formation of multi layer metal stack, the RTA process is used to establish chemical equilibrium. To ensure the formation of low resistivity ohmic contact, the thickness of M1, M2, M3, M4 and the RTA temperature must be optimized.

The goal of this study is to replace gold with other metals to reduce the cost of fabrication for GaN based devices. The function of gold is used as a cap layer to prevent oxidation. The metal to replace gold must be capable to prevent the oxidation. Furthermore, GaN based devices are used for high temperature operation, the metal choose for cap layer must also have high thermal stability. For this reason, this research choose tungsten as a cap layer to replace gold. Tungsten also benefits from its chemical stability hence can provide better long term reliability. And the diffusion barrier is no longer necessary in this ohmic contact structure.

Tungsten had been chosen to be the cap layer of this study because it has the highest melting point(3410°C) and one of the highest densities of all metals. It also has good strength at elevated temperatures.

But the oxide films become volatile above 538°C. WN_X/Cu layer was depotited on the top of Tungsten. As we know tungsten has already been used widely for Si ULSI technology as plug metal. It has good reliability and is compatiable to Si process.

3-3 TLM measurements

The equivalent circuit for TLM measurement is shown in Fig.3-1. Since the resistance of voltmeter is very large, the resistance of probe and the resistance between probe and metal can be neglected. Therefore the total resistance R_T can be calculated as:

$$R_T = 2Rcs + Rs = 2Rc + \frac{d \times \rho_{sh}}{Z}$$ [3-1]

Plot the R_T verse different d, the intercept of R_T and the slope represent -2Rc and $\dfrac{\rho_{sh}}{Z}$ respectively. And ρc can be calculated from

$$L_t = (\rho_c/\rho_{sh})^{1/2} \qquad\qquad\qquad [3\text{-}2]$$

3-4 Experimental procedure

The AlGaN/GaN heterosructure was grown on Si substrate using MOCVD technology. The carrier concentration and electron mobility obtained by Hall measurement were $1*10^{13}$ and $1600cm^2V^{-1}s^{-1}$, respectively. RCA clean process was carried before the process.

Mesa isolation of devices were formed by reactive ion etching (ICP-RIE) with chlorine based plasma. After that linear transfer length measurements (TLMS) test structure were patterned by photolithography. Prior to metal deposition, HCl was used to remove the native oxide on the wafer. The multi-layer metals were deposited by electron beam evaporation. The TLM patterns with spacing 3, 5, 10, 20, 35 um were patterned with standard lift-off process. Ti/Al/W metal stacks were fabricated with different thickness of Ti. After that the samples were annealed with designed temperature and time. The RTA temperatures range from 850 ^{o}C to 1000 ^{o}C for 30s. Multi-step annealing method was also used. First, the samples were annealed at 900 ^{o}C for 30s.After that increase the temperature to 950 ^{o}C and annealed again. Finally these contacts were annealed at 970 ^{o}C for 30s. The samples with best contact resistivity were prepared for TEM to understand the mechanism.

HP4142 was used to measure the current-voltage of TLM test structure and

calculated the contact resistance. The TEM samples were prepared by manual lapping. Ar-ion milling was used to finely polishing the specimens. AFM and X-ray were also used to analyze the structure.

3-5 Results and discussions

3-5-1 Contact resistivity with different thicknesses of Ti layer

The thickness is an important factor of ohmic contact. Different thickness of metals have different alloy composition. The thicknesses of W and Ti are fixed and the thickness of Ti range form 200 Å to 800 Å.The RTA temperatures range from 850 ^{o}C to 1000 ^{o}C for 30s.The results are shown in Fig. 3-1.

As shown in Fig. 3-1. Ti(200Å)/Al(1000 Å)/W(300 Å) has poor ohmic specific contact resistivity .The contact resistivity was quite high, about1.1×10^{-3} Ω cm^2. This is because there was no sufficient Ti to form Ti$_2$Al and AlTi. The remaining Al is unstable at high temperature since it's melting point is only 600°C. The excess Al tends to penetrate the surface of tungsten to react with oxygen and cause the degradation of surface morphology[7]. The oxidation is responsible for the high contact resistivity.

With increasing the thickness of Ti, the surface became flat with Ti(400Å)/Al(1000 Å)/W(300 Å) and contact resistivity is a little bit better than Ti(200Å)/Al(1000 Å)/W(300 Å). But the resistivity is still poor, about 8.2×10^{-4} Ω cm^2. As the thickness of Ti increase to 600 Å, the contact resistivity decrease to 3.1×10^{-4} Ω cm^2 after 970 ^{o}C annealing

Ti(800Å)/Al(1000 Å)/W(300 Å) annealed at 970 ^{o}C   has lowest contact resistivity which is similar to the result of Ti(600Å)/Al(1000 Å)/W(300 Å).

Most of the ohmic contacts research shows the best Ti:Al ratio to form the ohmic contact is 1:5 or 1:6. TiAlW ohmic contact has best contact resistance as Ti:Al= 1:2. This is because without the Ni/Au top layers, there must have sufficient Ti to react with Al. Lacking of Ti will cause the composition of alloy to change and the Al tends to ball up to the surface and results in degradation of the contact resistivity.

3-5-2 Annealing condition of Ti(600Å)/Al(1000 Å)/W(300 Å)

Ti/Al/W with 600 Å of Ti layer has the best resistance of four Ti thicknesses. Further annealing research was carried. Three types of annealing time: 30s, 60s and 120s were used and the contact resistivity as a function of temperature is shown in fig. 3-2. The samples after annealed for 60s showed best results for all of the temperature. After annealing at 970 ^{o}C for 60s, a specific contact resistivity of 3.6×10^{-5} Ω cm^2 was obtained.

3-5-3 Multi-step Annealing

In order to further decrease the specific contact resistivity, multi-step annealing was necessary. Qian Feng et al.[8] demonstrated a multi-step annealing process for Ti/Al/Ni/Au ohmic contacts. The concept is part of the alloys on the GaN surface were formed at low temperature. After that increasing the annealing temperature allows more Al diffuse to the GaN surface and create low work function TiAlN alloy.

In this work, three steps annealing was used for four thicknesses of Ti layer. The annealing temperatures were 900 ^{o}C, 920 ^{o}C, and 970 ^{o}C sequentially. The multi-step annealing results are presented in Fig. 3-3. The specific contact resistance was decrease drastically after multi step annealing. The comparison of contact resistivity

annealed with typical annealing and multi-step annealing process are presented in Fig. 3-4. Obvious trend can be observed that specific contact resistivity with multi-step annealing are much lower than typical annealing process for the four thicknesses of Ti layer.

As shown in Fig. 3-5, the I-V characteristic of Ti(600Å)/Al(1000 Å)/W(300 Å) is still nonlinear after 900 $^{\circ}$C annealing. After 900 $^{\circ}$C +920 $^{\circ}$C annealing the contact become ohmic but the slope is not good enough. The slope became more steep after further annealed with 970 $^{\circ}$C. The specific resistivity improved substantially to 2×10^{-5} Ω cm^2.

3-6 Material analysis

3-6 -1 Surface morphology

The flatness of ohmic contact is important since fabrication of compound semiconductor devices often involves specialized processes such as e-beam and lift-off lithography. The surface of Ti/Al/Ni/Au is very rough which has been an issue for photolithography. The roughness of traditionally Ti/Al/Ni/Au is about 100 nm, typically. This leads to the difficulty for precise photolithography.

Ti/Al/W contact has excellent surface morphology. The AFM images are show from Fig. 3-6. to Fig. 3-9 with different thicknesses after 900 $^{\circ}$C 30s annealing. The roughness is around 2~3nm. This result is excellent compared to other ohmic contact structures The AFM image of Ti/Al/Ni/Au was shown in Fig. 3-10. The roughness is 146.63nm which is much larger than Ti/Al/W contacts.

In this work the specific contact resistivity shows dependence with roughness as shown in Fig. 3-11. For the contacts with thinner Ti layers(200Å and 400Å) the contact resistivity are larger and the roughness are also larger. As the thickness

increased to 600 Å, the contact resistivity and roughness both decreased.

The surface morphology of Ti(600Å)/Al(1000 Å)/W(300 Å) annealed with temperatures ranging from 800 ^{o}C to 1000 ^{o}C are shown in Fig. 3-12 When temperature increased to 1000 ^{o}C, the specific contact resistivity increase rapidly. The roughness shows the same trend with contact resistivity. A further increase in annealing temperature resulted in the increase of contact resistance.

Ti(600Å)/Al(1000 Å)/W(300 Å) has very smooth surface morphology, the AFM images with different annealing temperature are shown in Fig. 3-13. to Fig. 3-17. As the results indicated the surface remain smooth after 950 ^{o}C annealing and the roughness increase slightly until 1000 ^{o}C.

3-6-2 X-ray diffraction

The XRD profiles are shown in Fig. 3-18. Four annealing conditions of the Ti(600Å)/Al(1000 Å)/W(300 Å) contacts were measured: sample A was as-deposited, sample B was annealed at 900 ^{o}C for30s, sample C was annealed at 900 ^{o}C 30s followed by annealed at 920 ^{o}C 30s, and sample D was annealed at 900C 30s ,920C 30s and 970s sequentially.

Ti and Al peaks were observed at the as deposited sample. With further annealing, Al$_2$Ti and AlTi peaks appeared both at sample B and C.

One interesting results is that peaks corresponding to Ti$_2$AlN and Al$_3$TiN were observed at sample D after three steps of annealing and the peaks from Al$_2$Ti and AlTi disappeared at the same time. This indicated that annealing at 970 ^{o}C caused significant phase transformation in Ti/Al metallic alloy. TiW also appeared in sample D. The phase change from Al$_2$Ti to AlTi$_3$ and the appearance of Ti2AlN could be the reason that resistivity drop at 970 ^{o}C as mentioned at previous chapter. The peak of tungsten become stronger from sample A to sample D which means recrystallined

15

may happen for W.

3-6-3 TEM images

The TEM pictures and EDS data of Ti (600 Å)/Al(1000 Å)/W(300 Å) before and after annealing were shown in Fig. 3-19 and Fig. 3-20. After annealing the surface morphology were still very flat. The Al and Ti alloy tends to ball up and penetrate through W surface. But 300 Å of W layer was enough to stop the penetration. Under the W surface, no oxygen was observed. This means W was a good cap layer to prevent oxidation. And there is no W diffusion observed thus the alloy reaction mechanism is less complicated than Ti/Al/Ni/Au. Ti diffused quickly to the position near W and formed $AlTi_3$ with Al. This alloy structure was also found on the surface of GaN. $AlTi_2$ existed between the $AlTi_3$ layers. As mentioned previously, XRD detected the $AlTi_3$ peak after multi-step annealing. The EDS data also support this result. Al_2TiN was found on the top of AlGaN surface.

3-7 WN_X/Cu Schottky contacts

The tungsten nitride films were deposited by reactive sputtering of pure tungsten target in Ar and N_2 atmosphere. The flow rates of the Ar and N_2 are 24 sccm and 5 sccm, respectively. The DC power for deposition was 200W with the pressure at 7.5×10^{-3} Torr. The copper layers were deposited with ebeam evaporation. The thickness of tungsten nitride was 500 Å and the thickness of copper was 1000 Å. The Schottky contacts of Ni/Au were also fabricated for comparison. The plot of current against voltage is shown in Fig. 3-29. The relation of forward current and applied voltage can be described by the equation:

$$I = I_0 \left[\exp\left(\frac{qV}{nkT}\right) - 1 \right] \tag{3-3}$$

$$I_0 = AA^{**}T^2 \left[\exp\left(\frac{-q\Psi b}{kT}\right) \right] \tag{3-4}$$

A is the area of Schottky contacts and Ψb is Schottky barrier height.

and equation 3-3 can be rewritten as:

$$I = I_0 \exp\left(\frac{qV}{nkT}\right) \left[1 - \exp\left(\frac{-qV}{kT}\right) \right] \tag{3-5}$$

and with natural logarithm on both sides, equation 3-5 becomes:

$$\ln\left[I / \left(1 - \exp\left(\frac{-qV}{kT}\right)\right) \right] = \frac{qV}{nkT} + \ln I_0 \tag{3-6}$$

From equation 3-6, the ideal factor could be extracted from the slope of plotting

$\ln\left[I / \left(1 - \exp\left(\frac{-qV}{kT}\right)\right) \right]$ versus V.

$$\text{Slope} = q/(nkT) \tag{3-7}$$

The schottky barrier height could be extracted by the y-axis intercept Y*.

$$\Psi b = \frac{kT}{q} \times \left[\ln(AA^{**}T^2) - Y^* \right] \tag{3-8}$$

The ideality factor of WN_X and Ni/Au were 1.57 and 1.41, respectively. The Schottky barrier height of Ni/Au was 0.61ev which was lower than the Schottky barrier height of WNx/Cu 0.67ev. That was the reason WN_X/Cu Schottky contacts had lower leakage current.

3-8 The evaluation of WN_X diffusion barrier

. It is widely known that the diffusion of copper will cause the degradation of devices. Proper design of diffusion barrier is usually necessary for copper metallization process. WN_X thin films were used for both ohmic and Schottky contacts as diffusion barriers in this research. The thickness of WN_X is 500 Å. The

multi layers of metals on the ohmic contacts were Ti/Al/W/WN$_X$/Cu. As for Schottky

contacts, WN$_X$/Cu multi layers were used. Both structures were annealed at 400°C for

30 minutes. The as-deposited samples and the annealed samples for both structures

were analyzed with auger electron microscope. The Fig. 30 and Fig. 31 show the

depth profile of Ti/Al/W/ WN$_X$ /Cu. The atomic percentage of copper decrease rapidly

through W. The depth profiles of WN$_X$ /Cu are shown in Fig. 32 and Fig. 33. The

copper diffused into the WN$_X$ layer and stop at the middle of WN$_X$ layer. The copper

didn't diffuse through metal layers in both Ti/Al/W/WN$_X$/Cu and WN$_X$ /Cu structures.

These results indicate that WN$_X$ with thickness of 500 Å is capable to stop copper

from diffusing into GaN.

3-9 Summary

In this chapter, the mechanism for the formation of Ti/Al/W ohmic contacts was

discussed. With multi-step annealing process a low contact resistivity of 2×10-5 was

obtained. The Ti/Al/W ohmic contacts showed better surface morphology compare to

Ti/Al/Ni/Au ones as shown in Fig 3-34 and 3-35. The mechanisms for the formation

of Ti/Al/W ohmic contacts were studied.

The WNx/Cu Schottky contacts were fabricated. An ideality factor of 1.57 and a

Schottky barrier height of 0.67 ev were observed. The characteristic of WNx/Cu

Schottky contacts is comparable with that of Ni/Au.
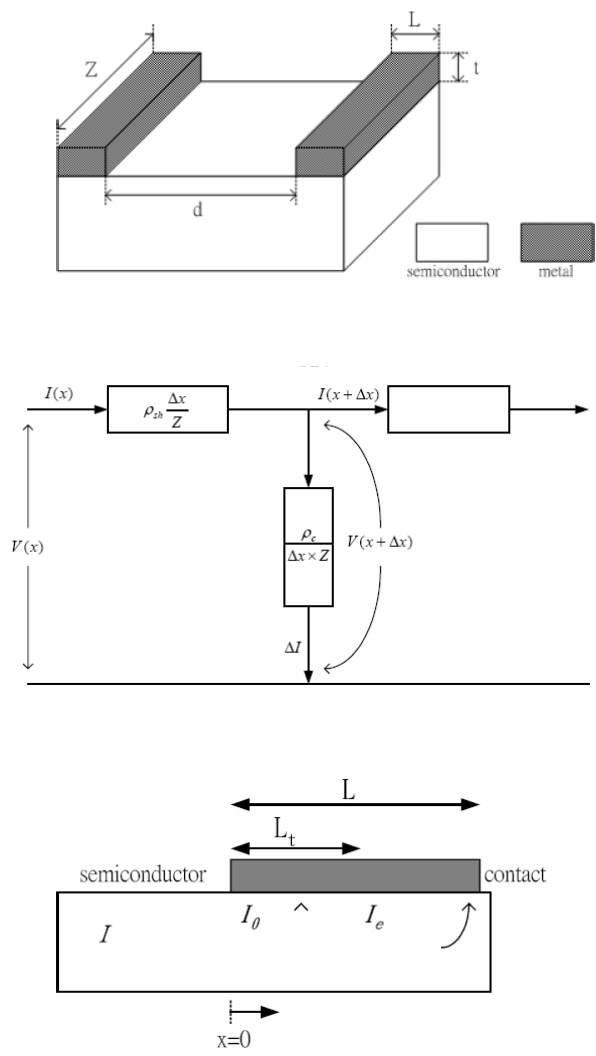
Figure 3-1 Equivalent circuit of TLM measurement
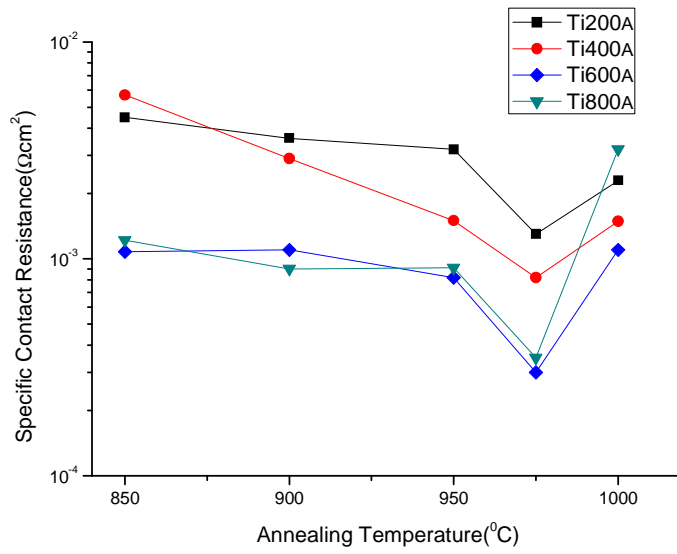
Figure 3-2. Contact resistivity as a function of annealing temperature with four different thicknesses of Ti layers.
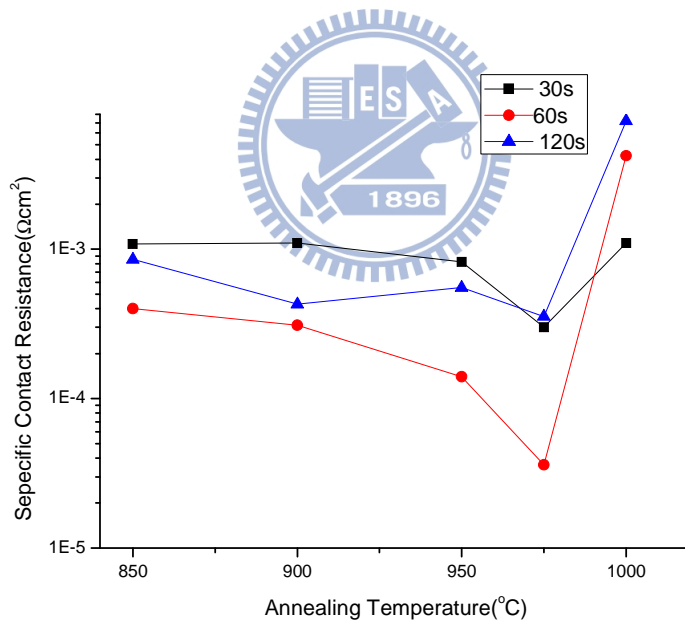
Figure 3-3. Contact resistivity of Ti(600Å)/Al(1000 Å)/W(300 Å) as a function of annealing temperature with four different annealing time
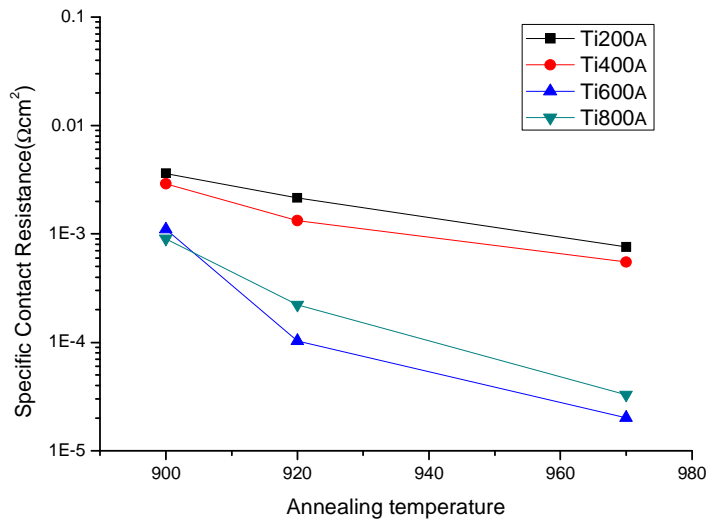
Figure 3-4. Contact resistivity annealed by multi-step annealing process as a function of temperature with four thickness of Ti layer.
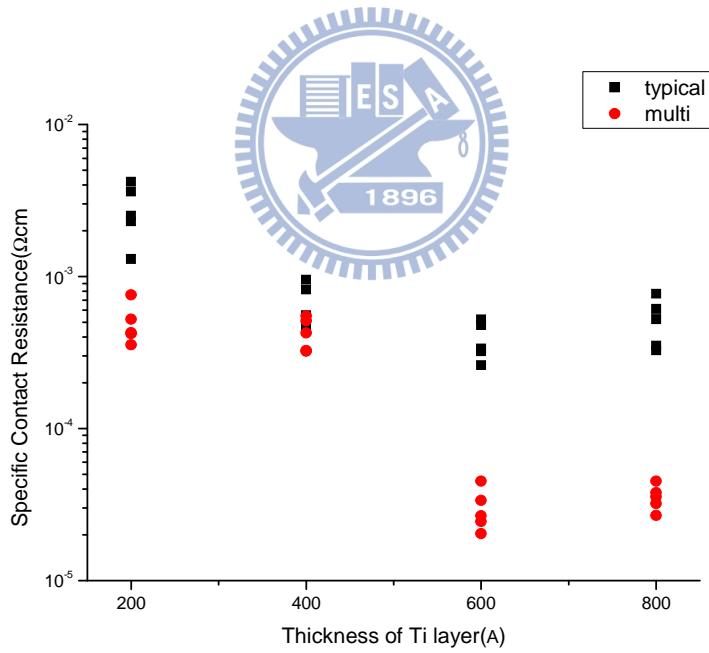
Figure 3-5. Comparison of contact resistivity with typical and multi-step annealing process
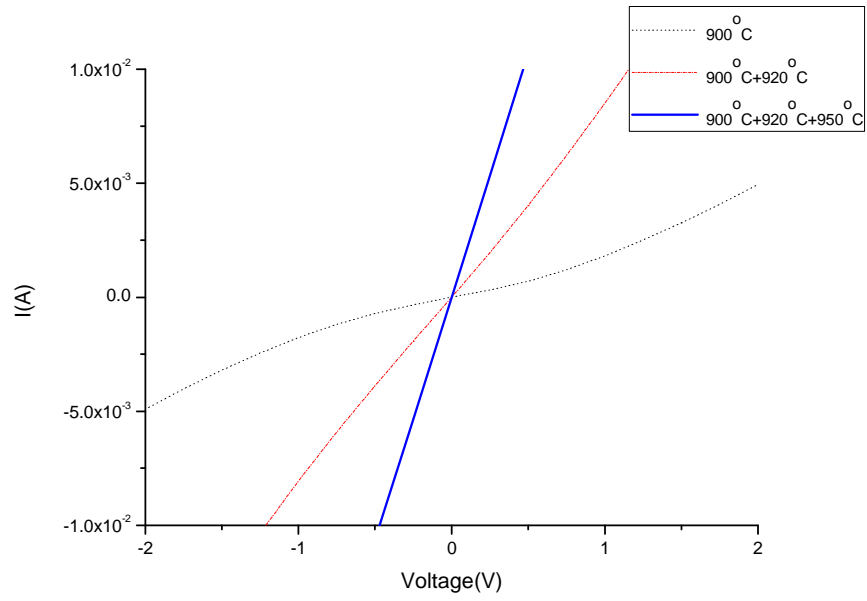
Figure 3-6. Current –voltage (I-V) characteristics of
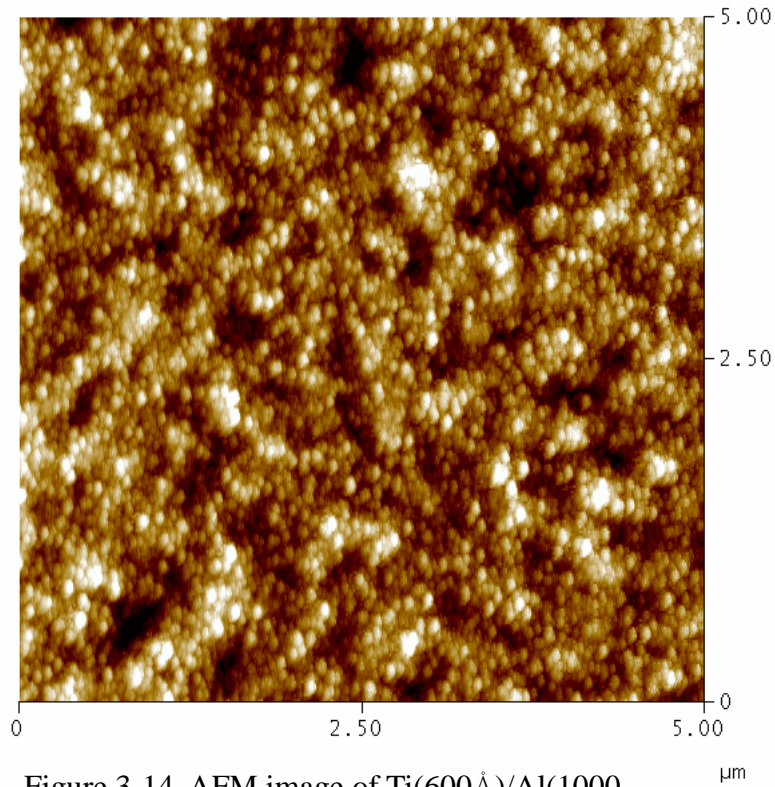Ti(600Å)/Al(1000 Å)/W(300 Å) with multi-step
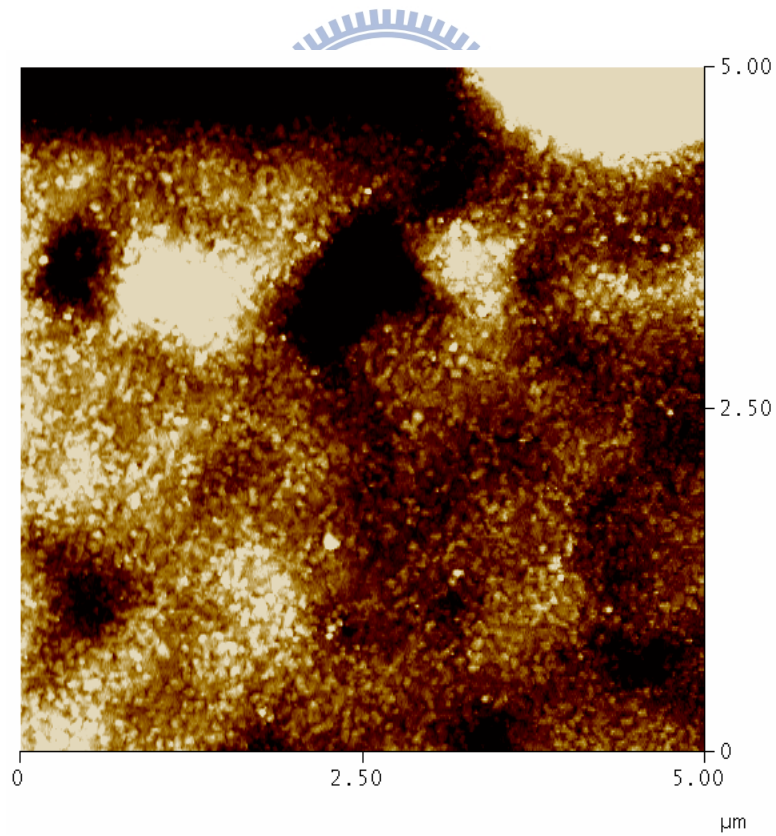
Figure 3-7. AFM image of Ti(200Å)/Al(1000
Å)/W(300 Å) after annealed at 900 °C 30s.
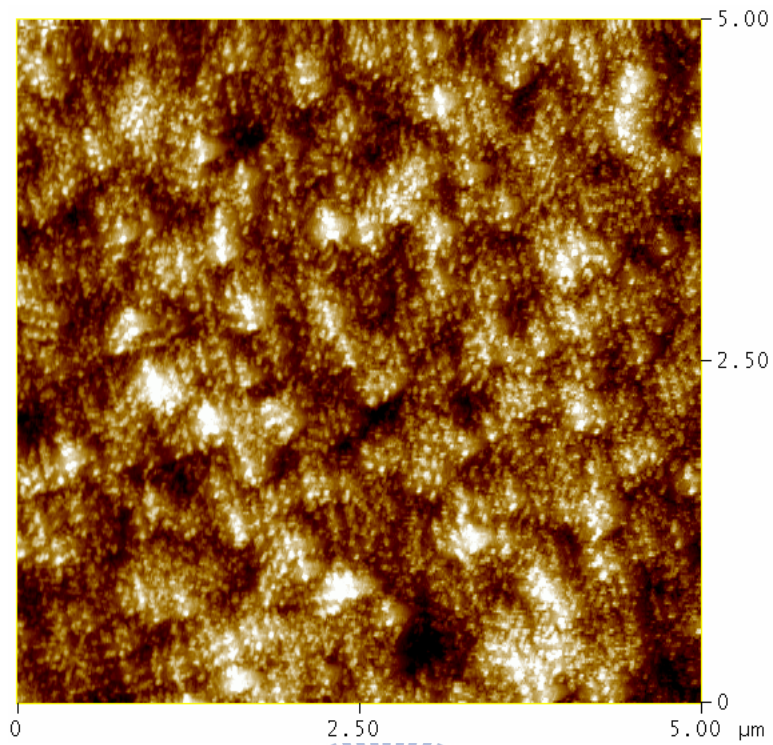
Figure 3-8. AFM image of Ti(400Å)/Al(1000
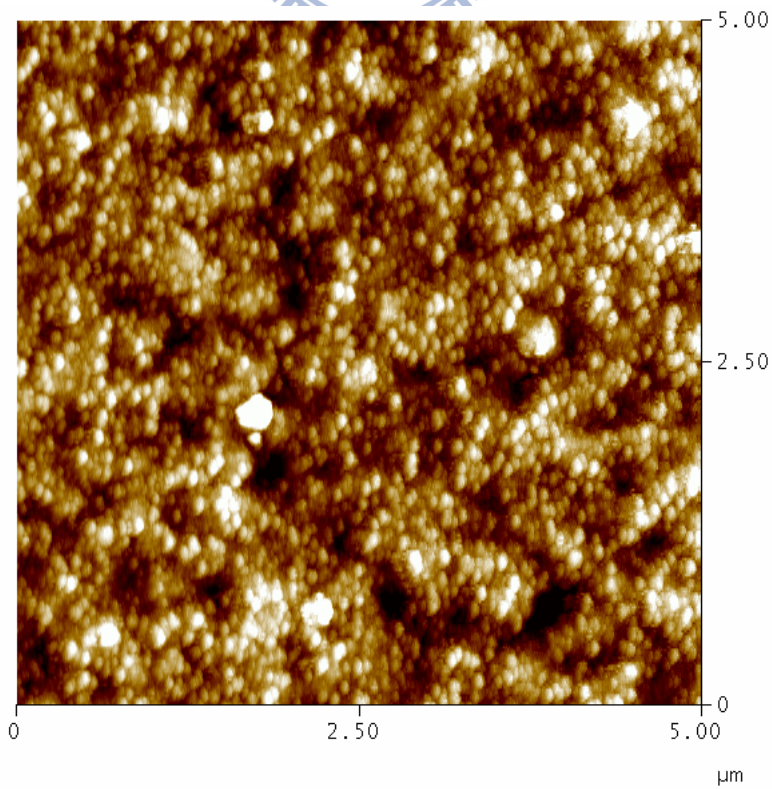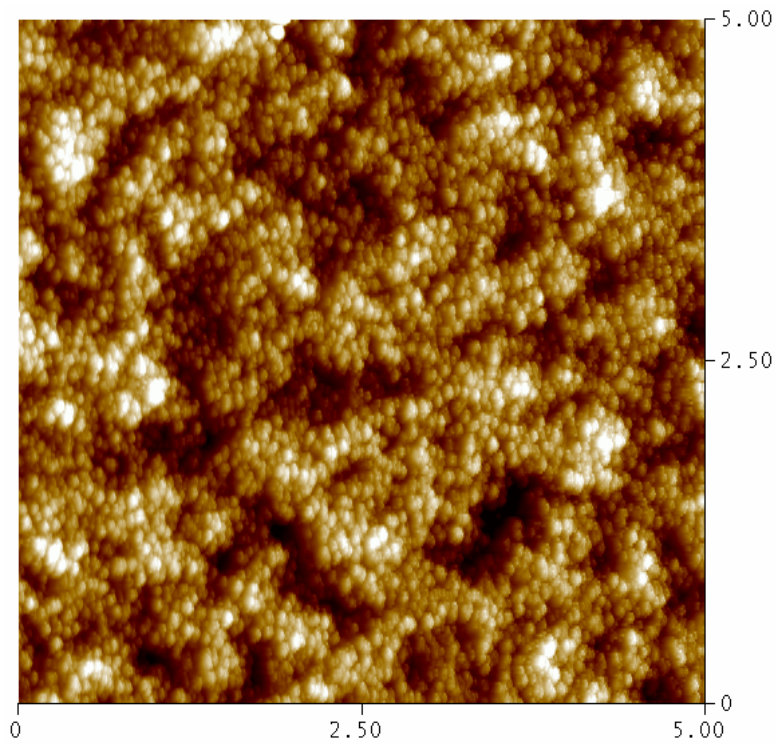Å)/W(300 Å) after annealed at 900 °C 30s.
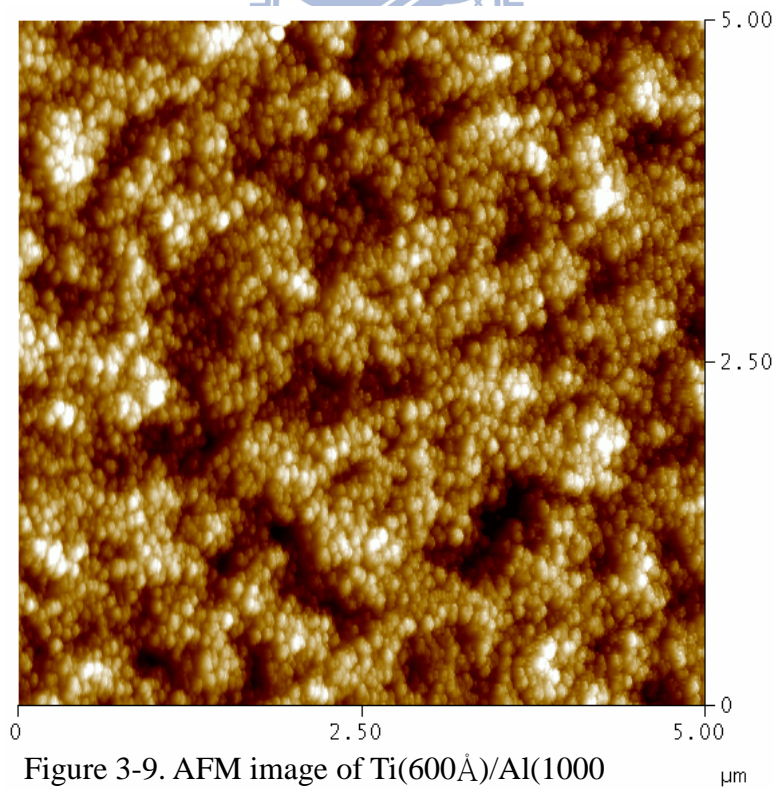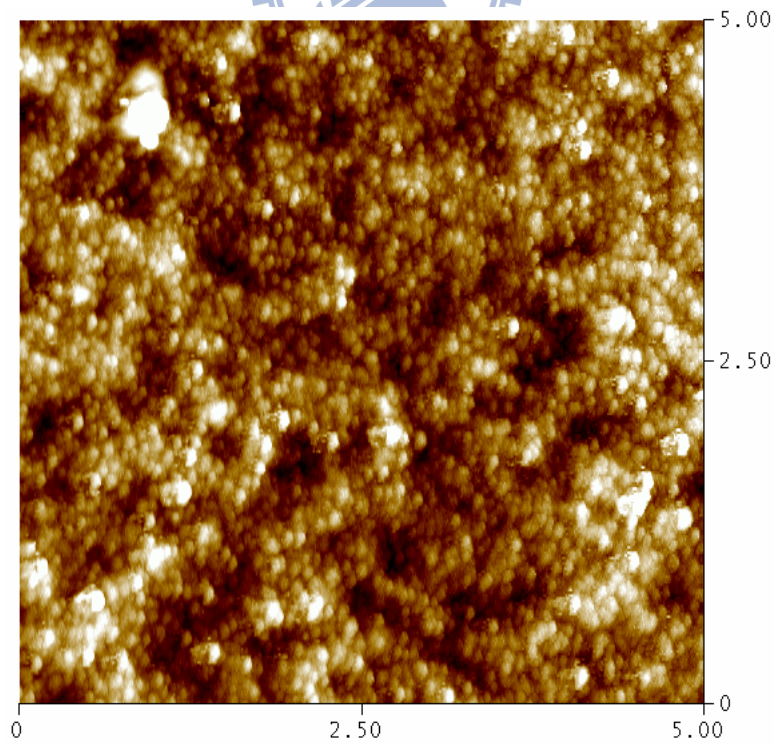

Figure 3-9. AFM image of Ti(600Å)/Al(1000
Å)/W(300 Å) after annealed at 900 °C 30s.
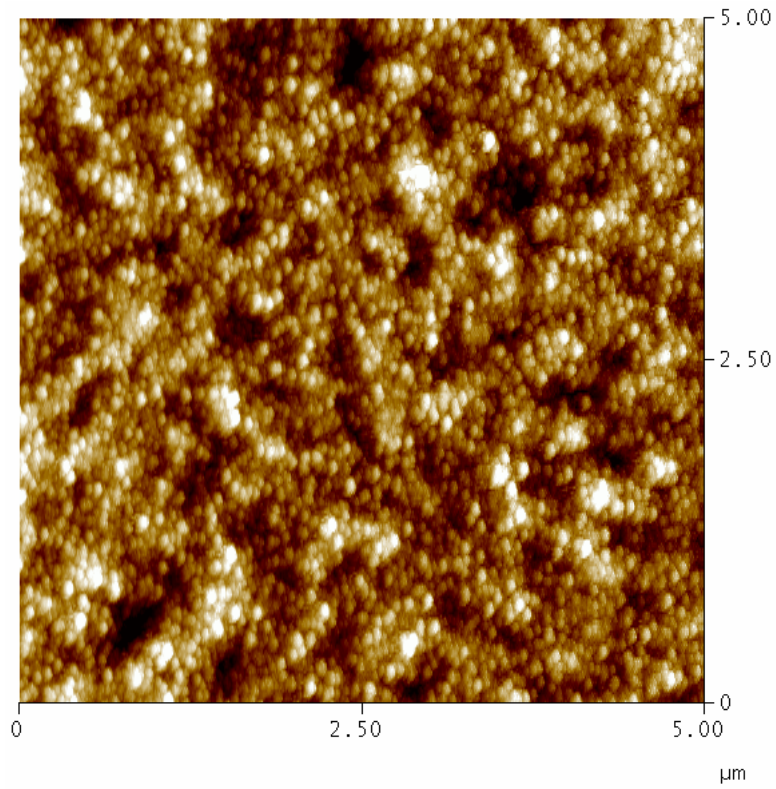
Figure 3-10. AFM image of Ti(800Å)/Al(1000 Å)/W(300 Å) after annealed at 900 ^{o}C 30s.
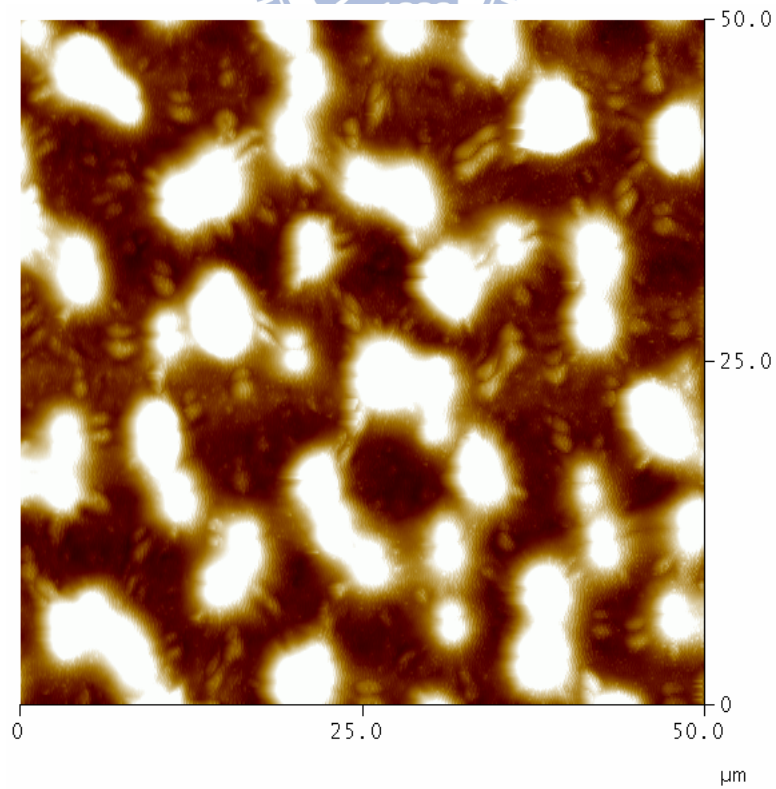
Figure 3-11. AFM image of Ti/Al/Ni/Au after annealed at 900 ^{o}C 30s.
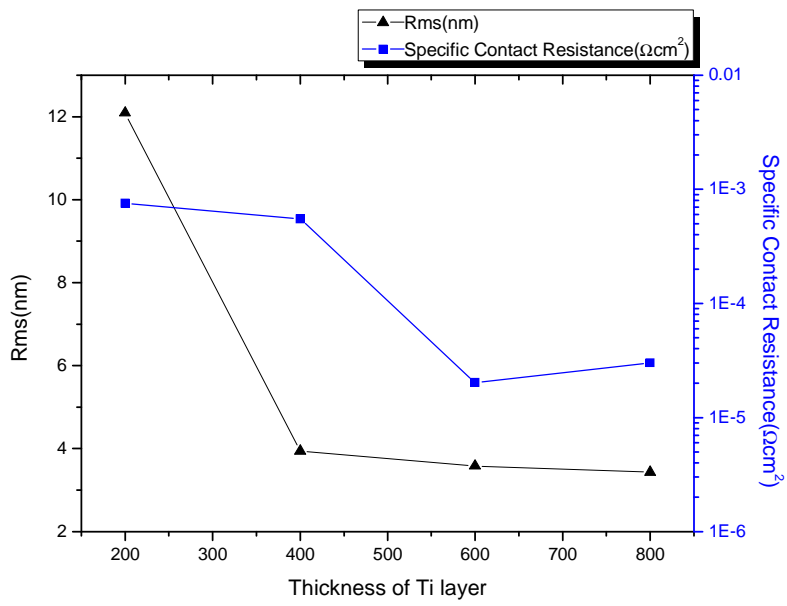
Figure 3-12. Rms and specific resistivity as function of Ti thickness.
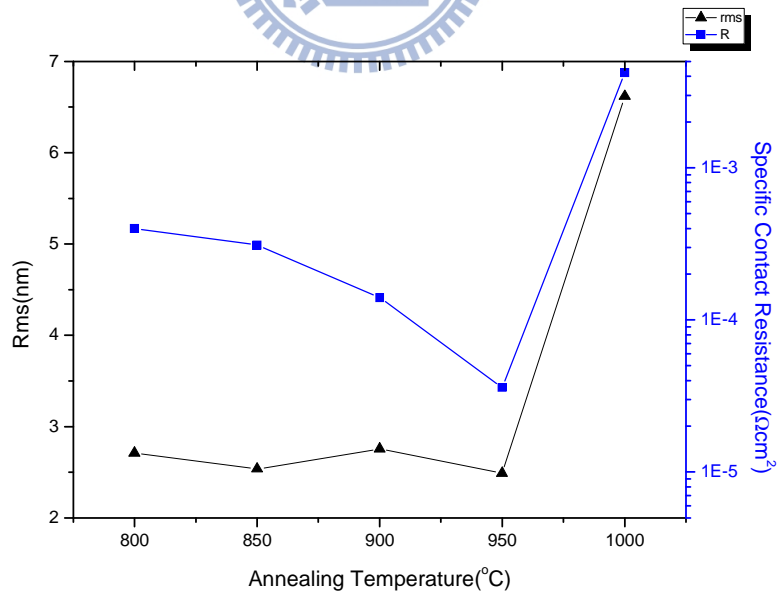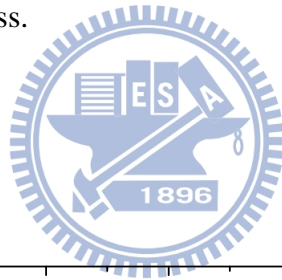
Figure 3-13. Rms and specific resistivity as function of annealing temperature

Figure 3-14. AFM image of Ti(600Å)/Al(1000 Å)/W(300 Å) after annealed at 800 ^{o}C 30s.

Figure 3-15. AFM image of Ti(600Å)/Al(1000 Å)/W(300 Å) after annealed at 850 ^{o}C 30s.

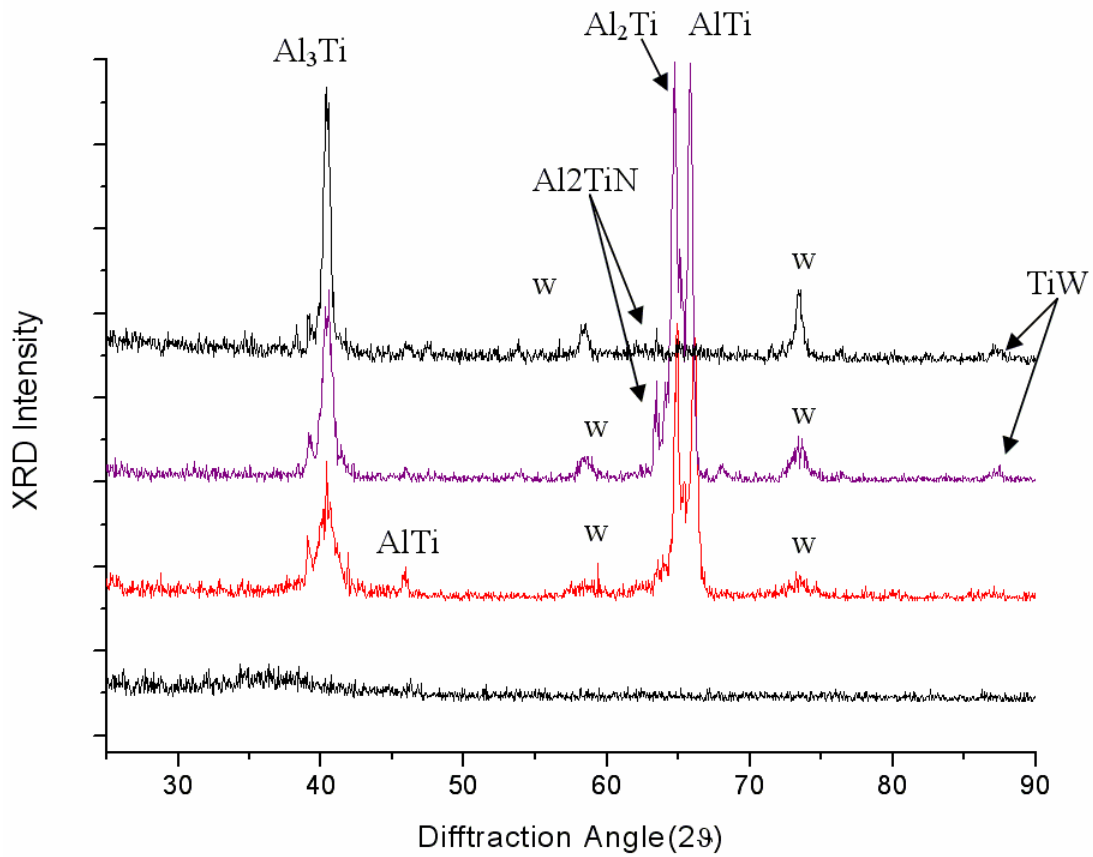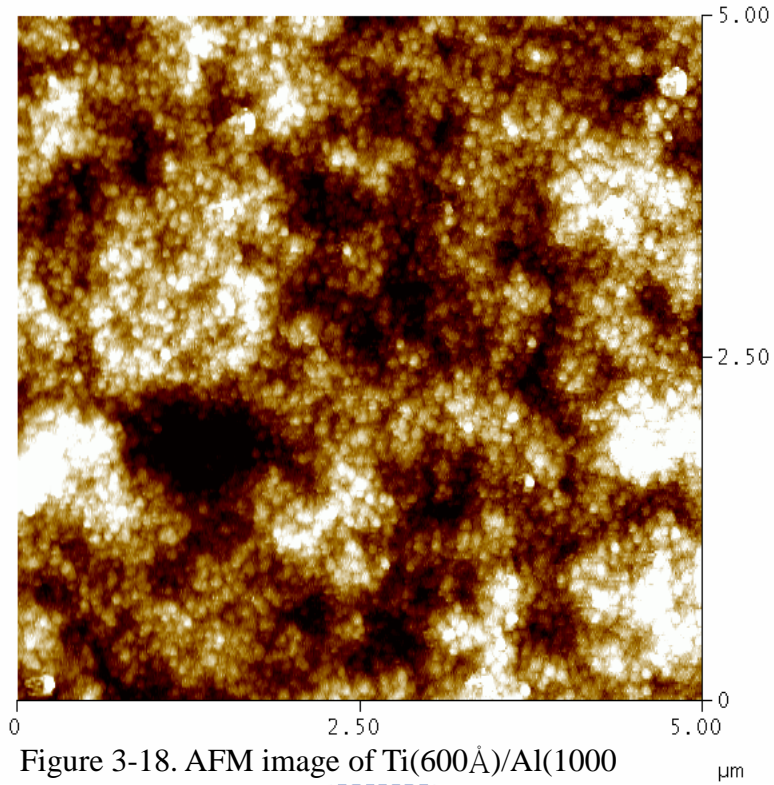Figure 3-16. AFM image of Ti(600Å)/Al(1000
Å)/W(300 Å) after annealed at 900 $^{\circ}$C 30s.

Figure 3-17. AFM image of Ti(600Å)/Al(1000
Å)/W(300 Å) after annealed at 950 $^{\circ}$C 30s.

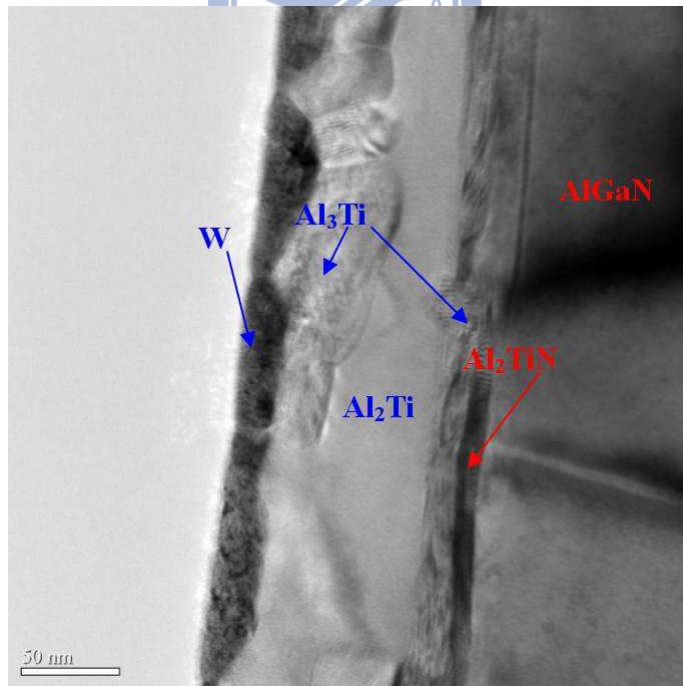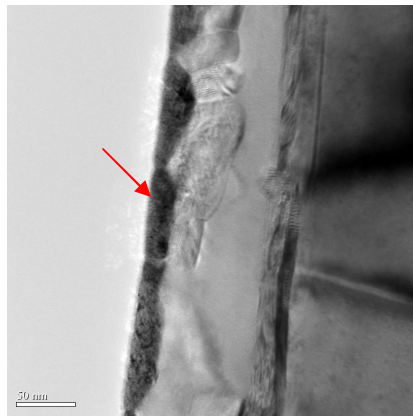Figure 3-18. AFM image of Ti(600Å)/Al(1000 Å)/W(300 Å) after annealed at 1000 ^{o}C 30s.

Figure 3-19. XRD scans of Ti(600 Å)/Al(1000 Å)/W(300 Å) with multi-step annealing.
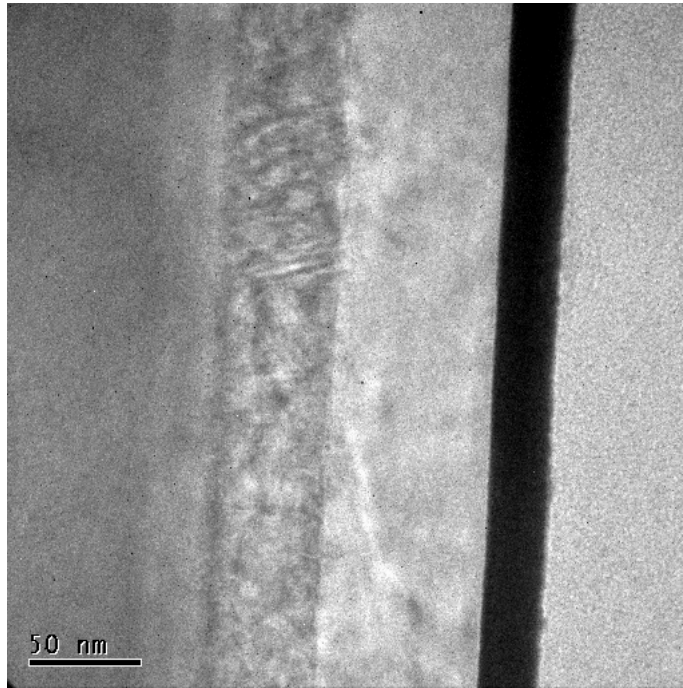
Figure 3-20. The TEM image of Ti(600Å)/Al(1000
Å)/W(300 Å) before annealing

Figure 3-21. The TEM image of Ti(600Å)/Al(1000
Å)/W(300 Å) after annealing

Element	Weight%	Atomic%
Ti	0.61	2.31
W	99.39	97.69
Totals	100.00	
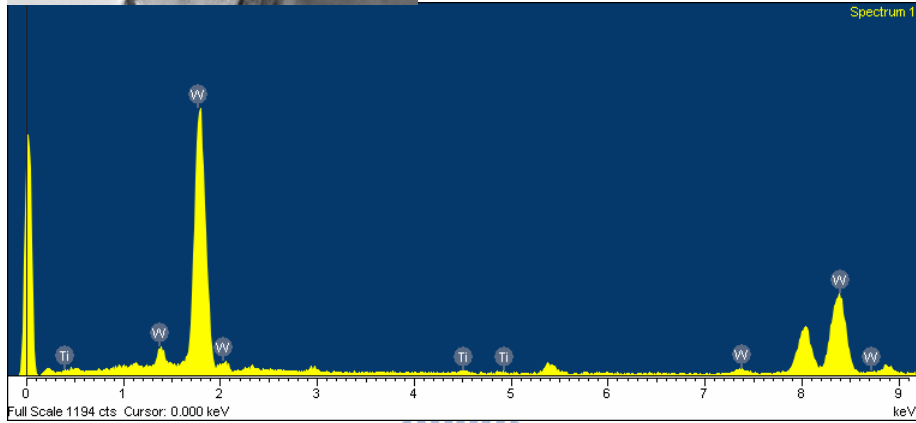
Figure 3-22. The TEM image of Ti(600Å)/Al(1000 Å)/W(300 Å) after annealing
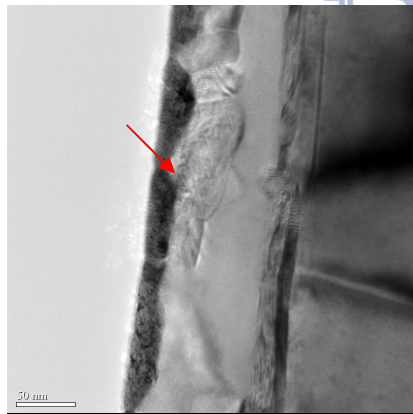
Element	Weight%	Atomic%
Al	25.11	37.31
Ti K	74.89	62.69
Totals	100.00	
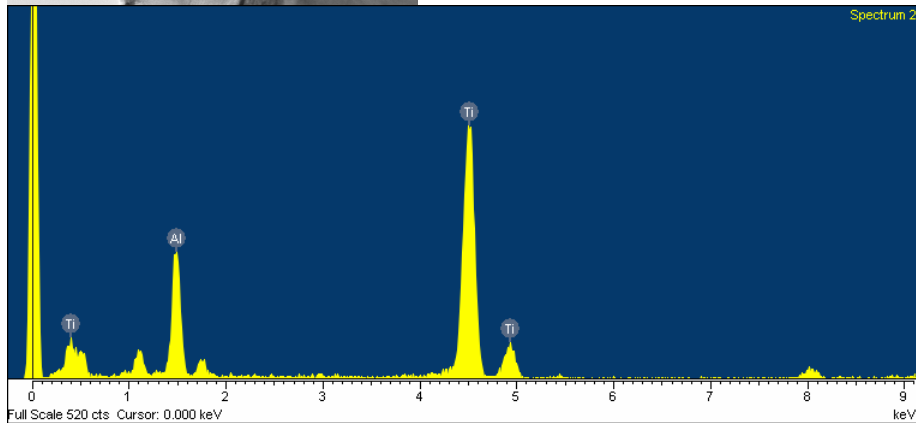
Figure 3-23. The TEM image of Ti(600Å)/Al(1000 Å)/W(300 Å) after annealing
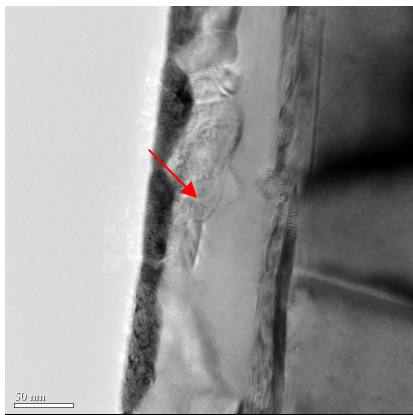
Element	Weight%	Atomic%
Al	20.90	32.40
Ti	73.74	64.39
Ga	5.36	3.22
Totals	100.00	
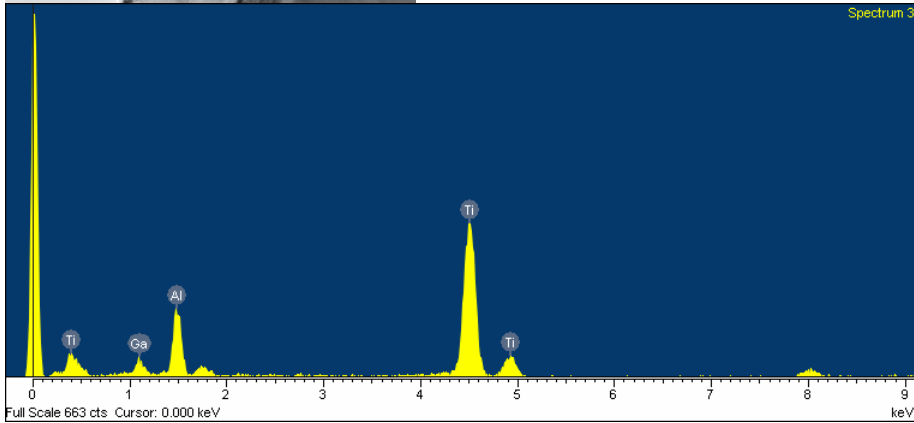
Figure 3-24. The TEM image of Ti(600Å)/Al(1000 Å)/W(300 Å) after annealing
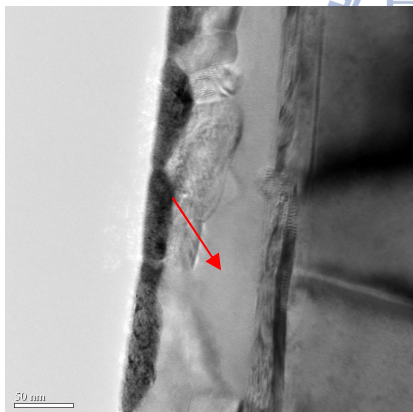
Element	Weight%	Atomic%
Al	49.78	64.51
Ti	45.09	32.92
Ga	5.13	2.57
Totals	100.00	
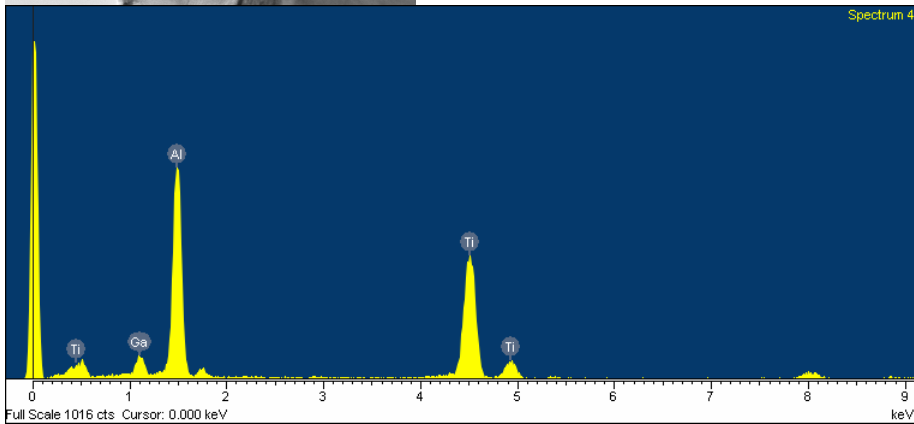
Figure 3-25. The TEM image of Ti(600Å)/Al(1000 Å)/W(300 Å) after annealing
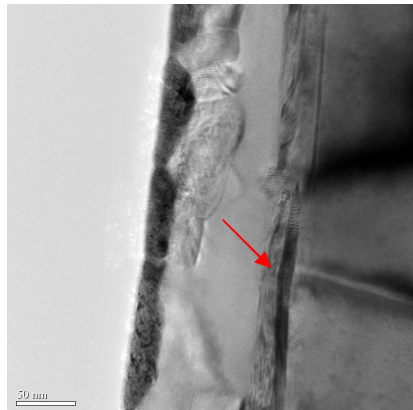
Element	Weight%	Atomic%
Al	18.32	28.96
Ti	75.61	67.33
Ga	6.07	3.71
Totals	100.00	
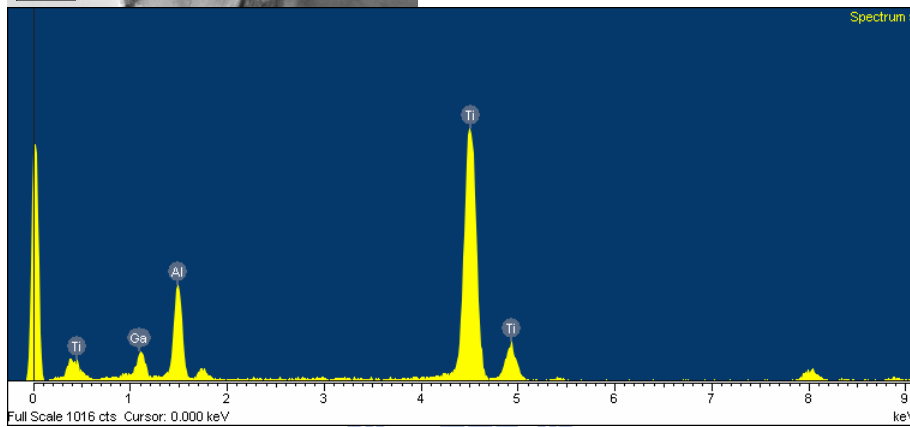
Figure 3-26. The TEM image of Ti(600Å)/Al(1000 Å)/W(300 Å) after annealing
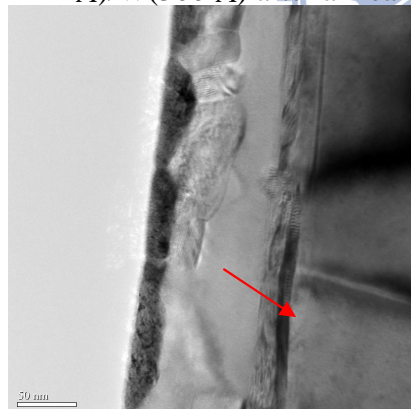
Element	Weight%	Atomic%
N	5.19	15.83
Al	15.20	24.04
Ti	40.86	36.41
Ga	38.75	23.72
Totals	100.00	
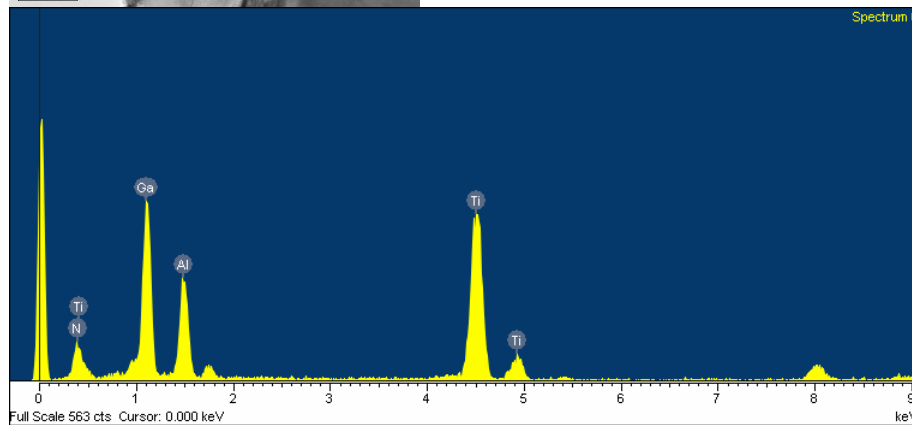
Figure 3-27. The TEM image of Ti(600Å)/Al(1000 Å)/W(300 Å) after annealing

Element	Weight%	Atomic%
N	9.22	32.07
Al	4.07	7.34
Ga	86.71	60.59
Totals	100.00	
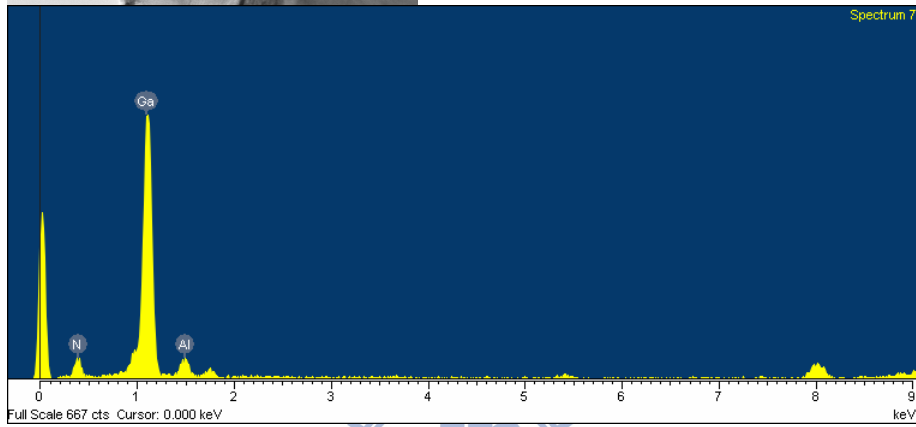
Figure 3-28. The TEM image of Ti(600Å)/Al(1000 Å)/W(300 Å) after annealing
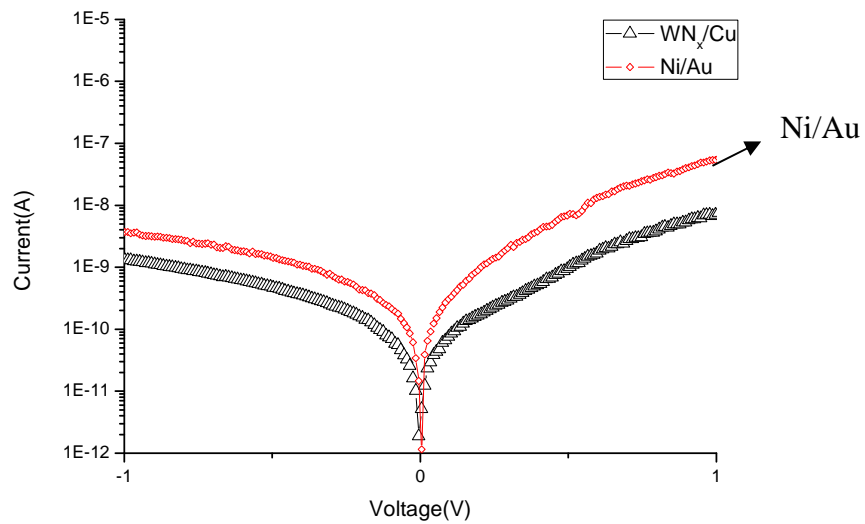
Figure 3-29.Current versus voltage of WN_x/Cu and Ni/Au Schottky contacts.
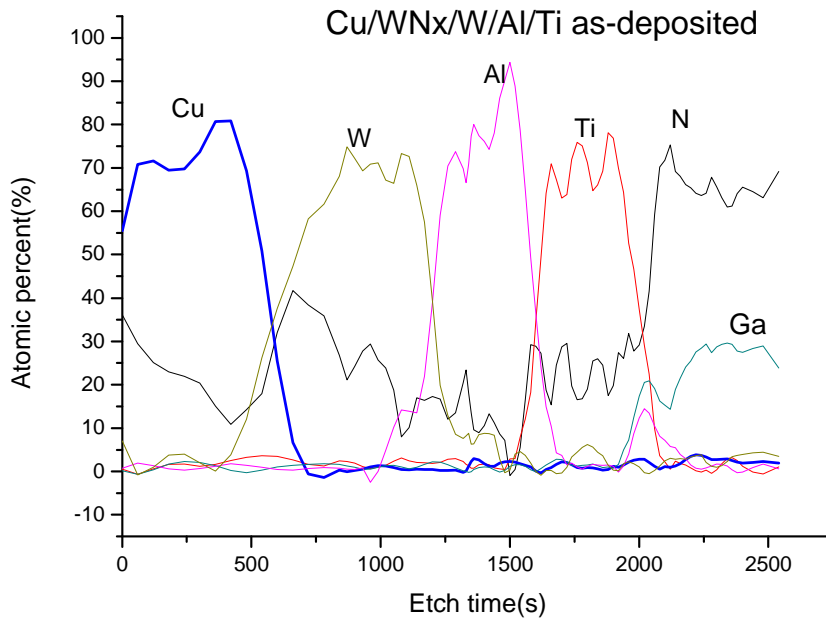
Figure 3-30 Auger depth profile of Cu/WN$_X$/W/Al/Ti as-deposited.
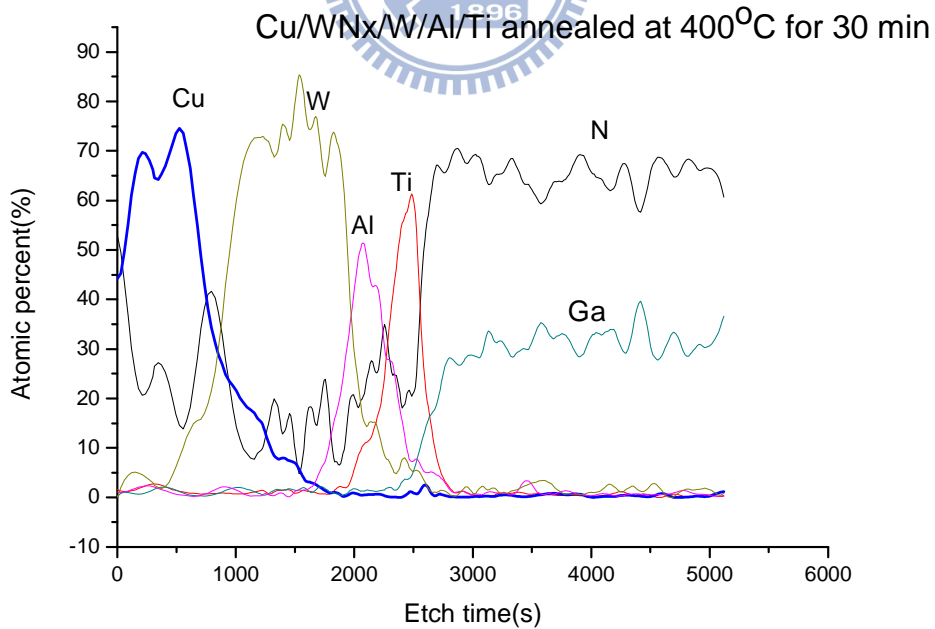
Figure 3-31 Auger depth profile of Cu/WN$_X$/W/Al/Ti annealed at 400°C for 30 minutes.

Figure 3-32 Auger depth profile of Cu/WN$_X$ as-deposited.

Figure 3-33 Auger depth profile of Cu/WN$_X$ annealed at 400°C for 30 minutes.

Figure 3-34 OM picture of Ti/Al/Ni/Au ohmic contact after annealed.

Figure 3-35 OM picture of Ti/Al/W ohmic contact after annealed

Chapter 4

Fabrication of AlGaN/GaN high electron mobility transistor with copper metallization process

4-1 Isolation

Isolation has several important fuctions:1 isolate devices from each other. 2 confine the current flowing through the desire path under the gate.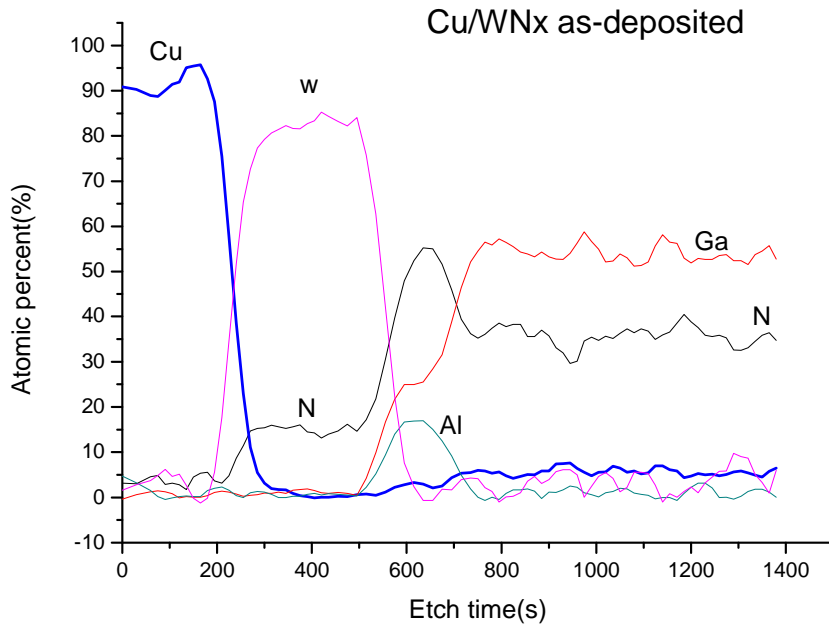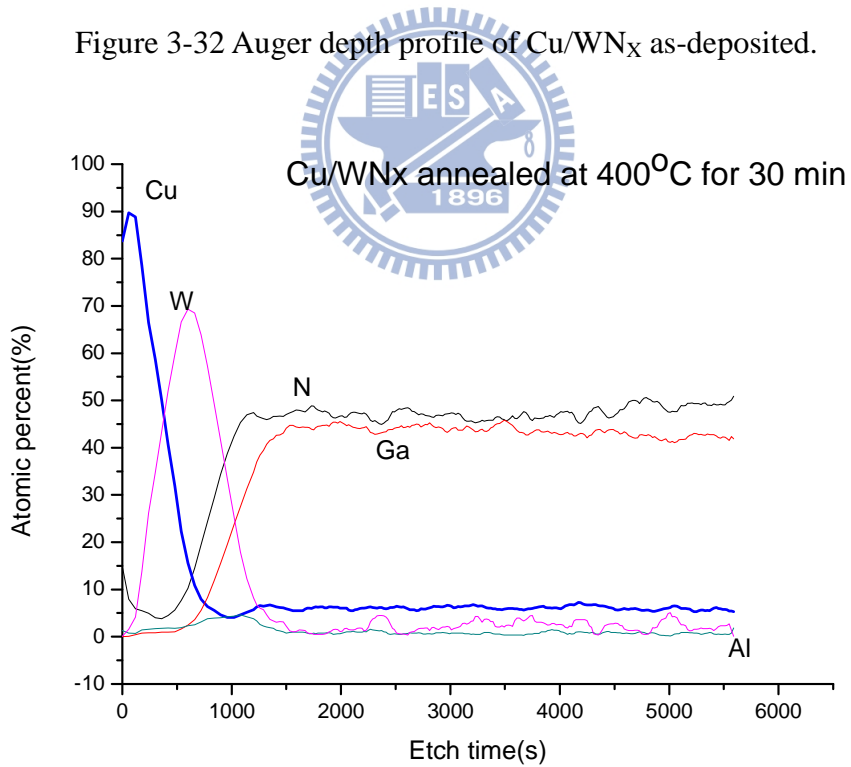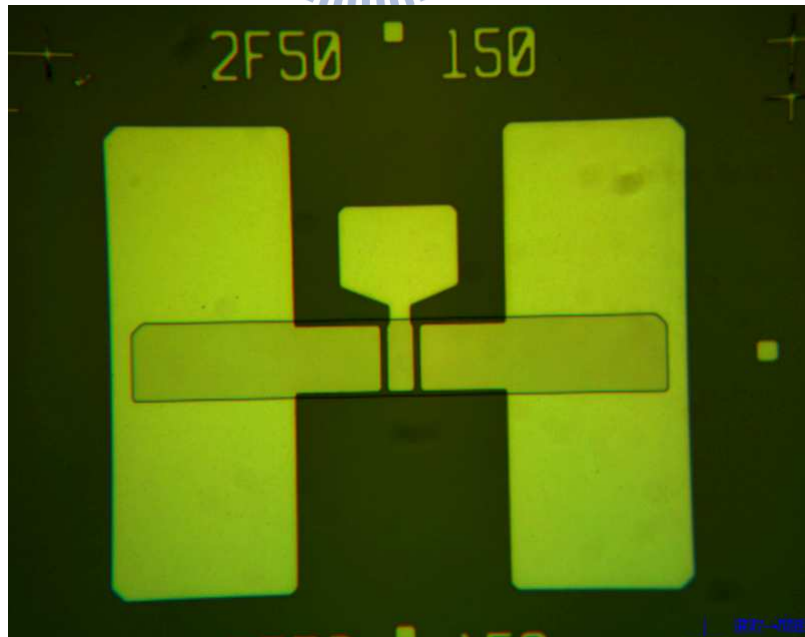 3 reduce the resistance and parasitic capacitance. There are two methods for isolation: ion implantation and etching the unused region of the devices. Wet etch need immerse AlGaN and GaN layer into solution and the edge is not as sharp as dry etch. This experiment use dry etch to define the isolation pattern. The etch depth for isolation is 2000Å to completely remove the 2DEG. The process was performed by ULVAC ICP system with Cl2 plasma and the power is 200W.

4-2 Ohmic contacts

Ti/Al/W multilayer metals were deposited after isolation using the standard lift off process. Ti/Al/Ni/Au metal stacks were fabricated for gold based devices. This research used E-beam evaporation to deposit Ti/Al followed by W deposition with sputter. The RTA process are performed in nitrogen atmosphere with multi-step annealing process as described in the previous chapter. The specific contact resistivity was obtained by TLM measurement.

4-3 Silicon nitride passivation

GaN is very sensitive and has many surface states. Oxidation and particulate

contamination can cause long term degradation. After formation of gate, a dielectric film was deposited to passivate the devices. This film prevent devices from chemicals, particles, humidity, and gases. Silicon nitride was used in this research. 1000 Å of silicon nitride was deposited on the devices using PECVD. The contact via was defined by photolithography and etch with RIE.

4-4 Gate formation and copper metallization

Az2020 photo resist was used to define the gate pattern. The clean surface is very important for Scotty contact. The sample was put into $HCl:H_2O = 1:10$ for 3 minutes to etch the native oxide. Gate foot prints was etched with ICP by CF_4 and O_2 plasma. The passivation layer on the region of ohmic contact was also etched. After that sputter was used to deposit WN_X 500 Å as diffusion barrier and gate metal. The power is 200W and the gas were Ar and N_2. The flow rate of Ar and N_2 were 24 and 5sccm, respectively. After that 1000Å of copper was deposited with E-beam evaporation. The same $WN_X(500 \text{ Å})/Cu(1000 \text{ Å})$ metal structure was deposited as the top layer of ohmic contact and gate metal.

4-5 DC Characteristics of AlGaN/GaN HEMTs with copper metallization

HP4142 was used to measure the DC characteristic of devices. Fig.4-1 shows the IV characteristic of the devices before passivation and the transconductance curve is plotted in the Fig. 4-3. The saturation current was 450mA/mm, the maximum Ids is 900 mA/mm and maximum transconductance was 126 mS/mm.

Fig. 4-2 shows the off-state breakdown measurement . A breakdown voltage of

125V was obtained. This is a high value with 2um gate and 5um source drain spacing. The result benefits from the large band gap nature of GaN material and the low leakage WN_X/Cu gate.

The DC characteristics of the devices after passivation are shown in Fig. 4-4 and 4-5.
The SiNx passivation was etched with CF_4 and O_2 plasma. In order to remove the SiN layer, over etch was necessary. CF_4 plasma tends to hit the surface of GaN and cause the effect called fluorine treatment which caused degradation of current and changed on-off properties . The device with passivation could be turned off at gate voltage of -3 V mean while the devices without passivation was turned off until -4V.

The devices with copper metallization were compared to gold based devices. The specific contact resistivity for copper based devices and gold based devices were 2×10^{-5} Ω cm^2 and 6.5×10^{-6} Ω cm^2, respectively. That is the reason Fig 4-5 shows the slope of on current for Au based devices is better than that of copper ones. This is because the specific contact resistivity of Ti/Al/Ni/Au is slightly better than Ti/Al/W. The saturation current of copper based devices is 450mA/mm and it is 420mA/mm for gold ones. The copper based devices showed broad shape of gm which is important for linearity. The maximum gm is 190 ms/mm and that of gold ones is 150 ms/mm as shown in Fig. 4-5. This results indicates that WN_x/Cu gate has better performance than Ni/Au ones.
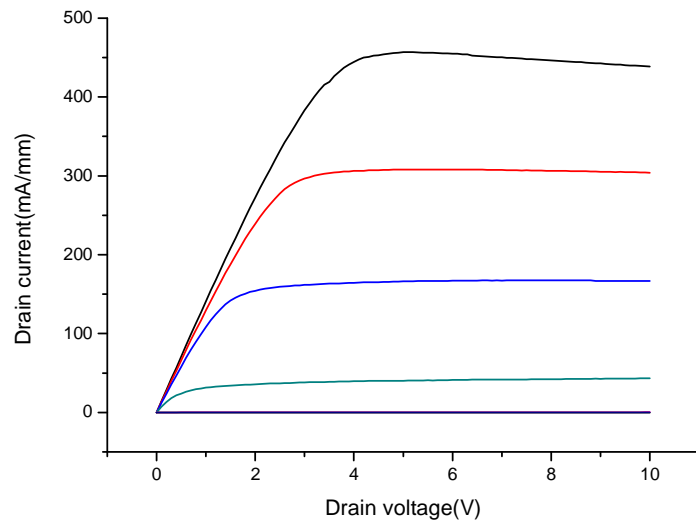
Figure. 4-1 IV characteristic of AlGaN/GaN HEMT
befor passivation. Vg =0~-5, step 1V

Figure. 4-2 Drain leakage current in the off-state.
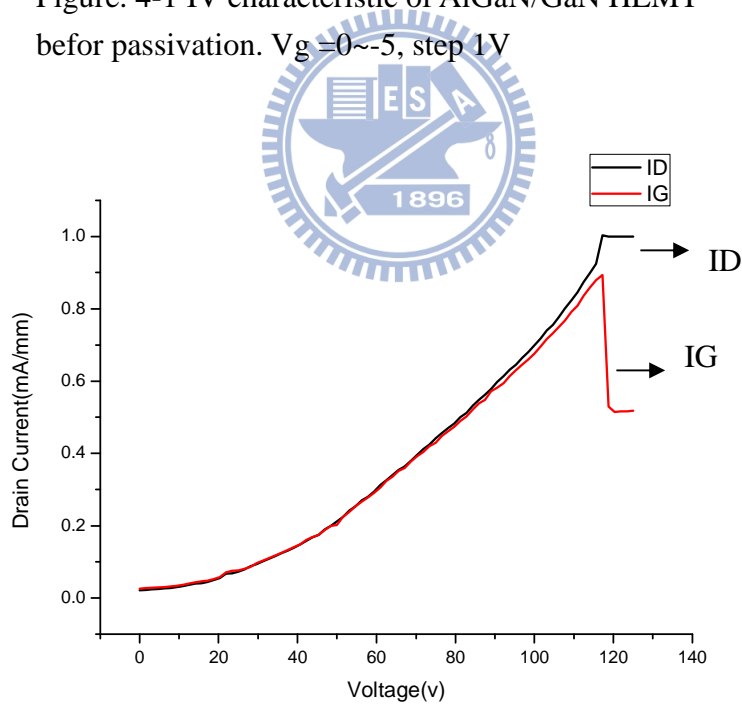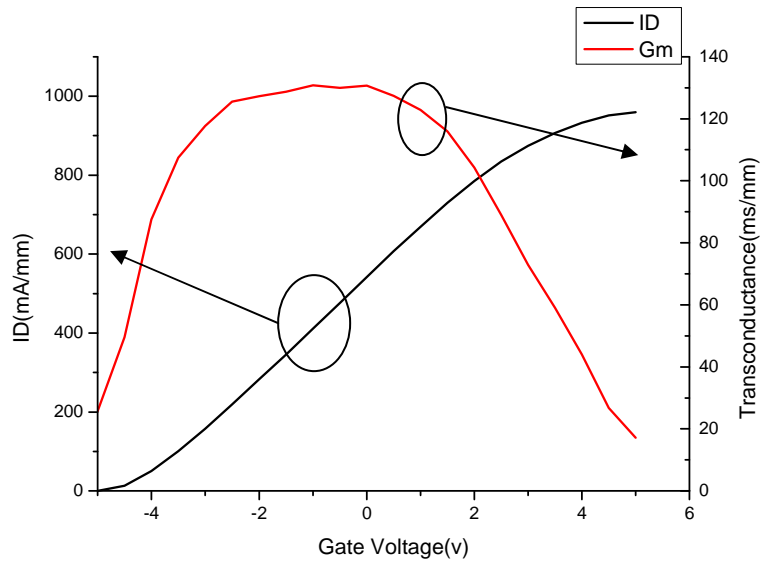
Figure. 4-3 Transconductance and Ids vesus gate voltage
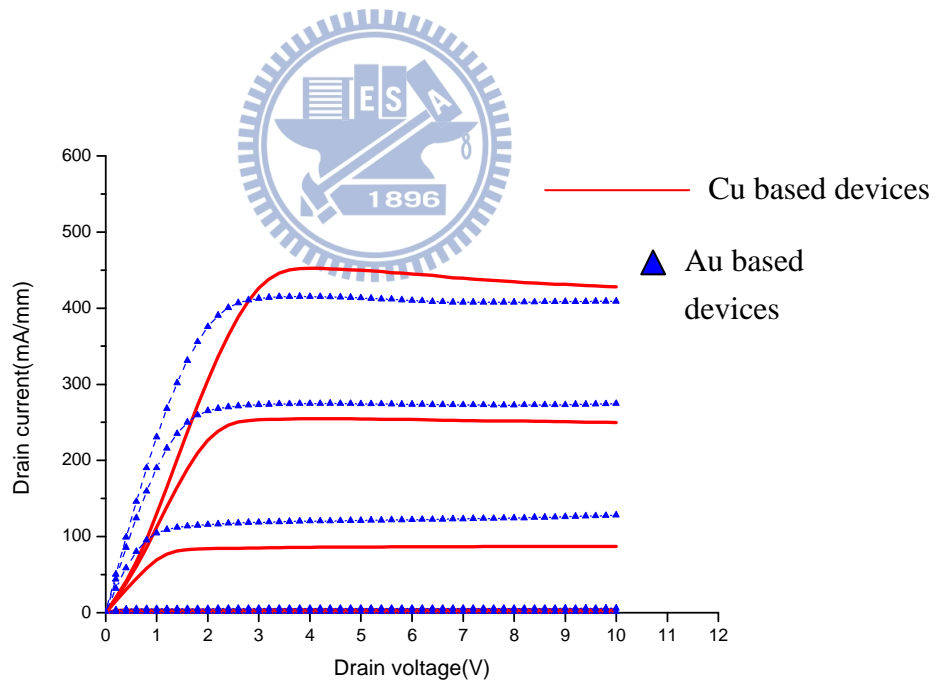of devices with copper metallization before passivation

Figure. 4-4 IV characteristic of AlGaN/GaN HEMT with
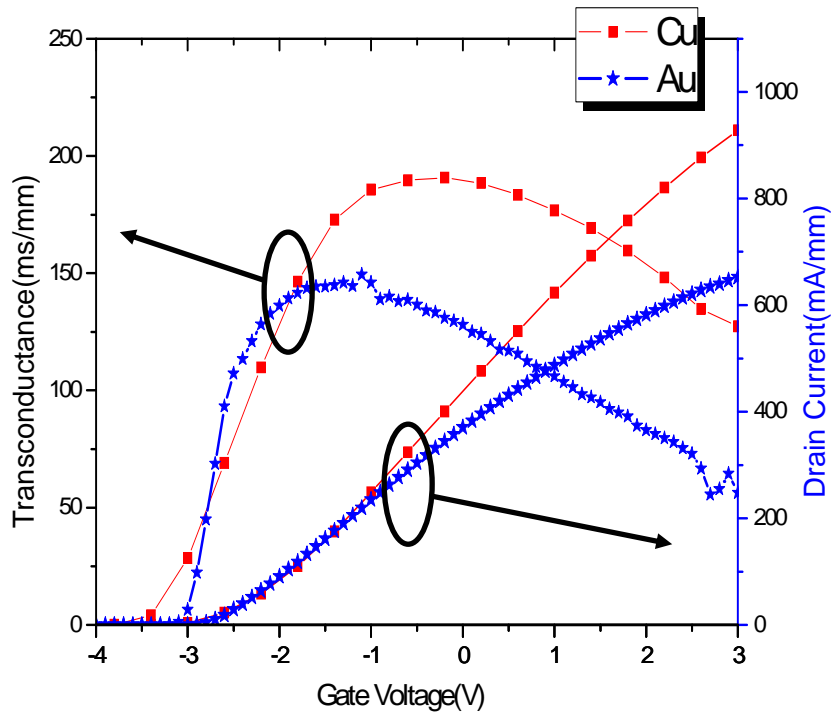copper metallization and gold metallization.

Figure. 4-5 Transconductance characteristic of
AlGaN/GaN HEMT with copper metallization.
The characteristic of gold based device was also
measured for comparison.

Chapter 5

Conclusions

The Ti/Al/W ohmic structures were fabricated for AlGaN/GaN HEMTs on Si substrates. With multi-step annealing process a specific contact resistivity of 2×10^{-5} Ω cm^2 was obtained. The mechanisms for the formation of ohmic contacts were studied with transmission microscope, AFM, and X-ray diffraction. Material analysis showed that tungsten could prevent Ti/Al alloy from penetrating the surface and keep the surface smooth. The formation of Ti$_2$AlN was observed when annealing temperature as high as 970°C. The Ti/Al alloy system also transformed from AlTi$_2$ to AlTi$_3$. The formation of Ti$_2$AlN and AlTi$_3$ should be the main reason of low specific contact resistivity for Ti/Al/W ohmic contacts. Ti/Al/W ohmic contacts also showed better surface morphology compared with Ti/Al/Ni/Au.

The WNx/Cu multi layers were fabricated as Schottky contacts. An ideality factor of 1.57 and Schottky barrier height of 0.67ev were observed.

The devices with copper metallization and gold metallization were both fabricated. Although copper based devices with the on resistance larger than gold ones, the other electrical properties such as maximum transconductance, and saturation current are all better than that of gold based devices. Almost the same devices performance were achieved with 20~30% of cost reduction. This indicates that the process developed in this research is suitable for low cost AlGaN/GaN HEMTs process on Si substrate.

References

[1] H. Morkoc and S. N. Mohammad, Science 267, 51 (1995)

[2] N. A. Papanicolaou, M. V. Rao, J. Mittereder, and W. T. Anderson, J. Vac. Sci. Technol.B 19, 261 (2001).

[3] V. Kumar, L. Zhou, D. Selvanathan, and I. Adesida, J. Appl. Phys. 92, 1712 (2002)

[4] Z. M Zhao, R. L. Jiang, P. Chen, D. J. Xi, Q. H. Yu, B. Shen, R. Zhang, Appl. Phys. Lett. 79 218 (2001)

[5] C. t. Lee and H. W. Kao, Appl. Phys. Lett. 76,2364 (2000)

[6] A. Motayed, R. Bathe, M. C. Wood, O. S. J. Appl. Phys. 93, 1087 (2003)

[7] S. Noor Mohammad J. Appl. Phys. 95, 7940 (2004)

[8] Qian Feng, Li-Mei Li, Yue Hao. Solid State Electronics. 53, 955 (2009)

[9] V. Kumar, W. Lu, F. A. Khan, R. Schwindt, A. Kuliev, G. Simin, J. Yang, M. Asif and I. Adesida, Electron. Lett. 38, 252 (2002)

[10] M. Higashiwaki, T. Mimura and T. Matsui, Japanese Journal of Applied Physics. 45, L1111 (2006).

[11] Y.-F. Wu, A. Saxler, M. Moore, R.P. Smith, S. Sheppard, P.M. Chavarkar, T. Wisleder, U.K. Mishra, and P. Parikh, IEEE Electron. Dev. Lett. 25, 117 (2004).

[12] S. Ruvimov et al., Appl. Phys. Lett. 69, 1556 (1996).

[13] S. C. Binari, H. B. Dietrich, G. Kelner, L. B. Rowland, K. J. Doverspike, and D. K. Wickenden, J. Appl. Phys., 78, 3008 (1995).

[14] S. J. Pearton, C. B. Vartuli, J. C. Zolper, C. Yuan, and R. A. Stall, Appl. Phys. Lett. 67, 1435 (1995)

[15] B. Boudart, Y. Guhel, J. C. Pesant, P. Dhamelincourt, and M. A. Poisson, J. Phys. 49, 021001 (2004)

[16] S. J. Pearton, J. C. Zolper, R. J. Shul, and F. Ren, J. Appl. Phys. 94, 1662 (2003.)

[17] Y. Kokubun, T. Seto, and S. Nakagomi, Jpn. J. Appl. Phys. Part 2. 40, L663 (2001).

[18] Z. Lin, H. Kim, J. Lee, and W. Lu, Appl. Phys. Lett. 84, 1585 (2004)

[19] T. Nakayama, Appl. Phys. Lett. 85, 2 (2004)

[20] Y. F. Wu et al., IEEE Electron Device Lett. 25, 117 (2004).

[21] V. Kumar, W. Lu, R. Schwindt, A. Kuliev, G. Simin, J. Yang, M. Asif Khan, and I. Adesida, IEEE Electron Device Lett. 23, 455 (2002).

[22] P. Neudeck, R. S. Okojie, and L. Y. Chen, Proc. IEEE 90, 1065 (2002).

[23] R. J. Trew, G. L. Bilbro, W. Kuang, Y. Liu, and H. Yin, IEEE Microw. 6, 56 (2005).

[24] B. Jacobs, M. C. J. C. M. Kramer, E. J. Geluk, and F. Karouta, J. Cryst. Growth 241, 15 (2002)

[25] D. Qiao, Z. F. Guan, J. Carlton, S. S. Lau, and G. J. Sullivan, Appl. Phys. Lett. 74, 2652 (1999).

[26] F. M. Mohammed, L. Wang, I. Adesida, and E. Piner: J. Appl. Phys. 100, 023708 (2006).

[27] L. Wang, F. M. Mohammad, and I. Adesida, J. Appl. Phys. 98, 106105 (2005).

[29] A. N. Bright, P. J. Thomas, M. Weyland, D. M. Tricker, C. J. Humphreys, and R. Davies: J. Appl. Phys. 89, 3143 (2001)

[30] D. Selvanathan, L. Zhou, V. Kumar, I. Adesida, and N. Finnegan, Journal of Electronic Materials. 32, 335 (2003)